DR. 111

DSE/2538-3

DEVELOPMENT OF A THIN FILM POLYCRYSTALLINE SOLAR CELL FOR LARGE SCALE TERRESTRIAL USE

Quarterly Progress Report, January 1—March 31, 1977

July 1977

Work Performed Under Contract No. EX-76-C-01-2538

Institute of Energy Conversion
University of Delaware
Newark, Delaware

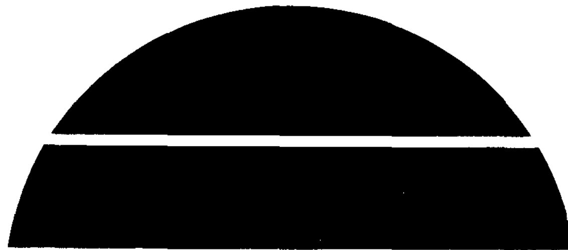

MASTER

U.S. Department of Energy

Solar Energy

DISTRIBUTION OF THIS DOCUMENT IS UNLIMITED

DISCLAIMER

This report was prepared as an account of work sponsored by an agency of the United States Government. Neither the United States Government nor any agency thereof, nor any of their employees, makes any warranty, express or implied, or assumes any legal liability or responsibility for the accuracy, completeness, or usefulness of any information, apparatus, product, or process disclosed, or represents that its use would not infringe privately owned rights. Reference herein to any specific commercial product, process, or service by trade name, trademark, manufacturer, or otherwise does not necessarily constitute or imply its endorsement, recommendation, or favoring by the United States Government or any agency thereof. The views and opinions of authors expressed herein do not necessarily state or reflect those of the United States Government or any agency thereof.

DISCLAIMER

Portions of this document may be illegible in electronic image products. Images are produced from the best available original document.

NOTICE

This report was prepared as an account of work sponsored by the United States Government. Neither the United States nor the United States Department of Energy, nor any of their employees, nor any of their contractors, subcontractors, or their employees, makes any warranty, express or implied, or assumes any legal liability or responsibility for the accuracy, completeness or usefulness of any information, apparatus, product or process disclosed, or represents that its use would not infringe privately owned rights.

This report has been reproduced directly from the best available copy.

Available from the National Technical Information Service, U. S. Department of Commerce, Springfield, Virginia 22161.

Price: Paper Copy $6.00
Microfiche $3.00

DSE/2538-3
Distribution Category UC-63e

DEVELOPMENT OF A THIN FILM POLYCRYSTALLINE SOLAR CELL FOR LARGE SCALE TERRESTRIAL USE

Quarterly Progress Report

January 1, 1977 - March 31, 1977

E(49-18)-2538

July 1977

NOTICE
This report was prepared as an account of work sponsored by the United States Government. Neither the United States nor the United States Department of Energy, nor any of their employees, nor any of their contractors, subcontractors, or their employees, makes any warranty, express or implied, or assumes any legal liability or responsibility for the accuracy, completeness or usefulness of any information, apparatus, product or process disclosed, or represents that its use would not infringe privately owned rights.

INSTITUTE OF ENERGY CONVERSION

UNIVERSITY OF DELAWARE

NEWARK, DELAWARE 19711

Supported by the Energy Research and Development Administration

DISTRIBUTION ...

BIBLIOGRAPHIC DATA SHEET	1. Report No. E(49-18)-2538 PR 77/1	2.	3. Recipient's Accession No.
4. Title and Subtitle Development of a Thin Film Polycrystalline Solar Cell for Large Scale Terrestrial Use			5. Report Date July 1977
			6.
7. Author(s)			8. Performing Organization Rept. No.
9. Performing Organization Name and Address Institute of Energy Conversion University of Delaware Newark, Delaware 19711			10. Project/Task/Work Unit No.
			11. Contract/Grant No. E(49-18)-2538
12. Sponsoring Organization Name and Address Division of Solar Energy Energy Research and Development Administration 20 Massachusetts Avenue, N. W. Washington, DC 20545			13. Type of Report & Period Covered 1/1/77 - 3/31/77
			14.
15. Supplementary Notes			

16. Abstracts

Maximum power conversion efficiency in actual sunlight for the CdS/Cu_2S cell has reached 8.55% and short circuit currents of 25.0 mA/cm^2 have been measured.

The $(CdZn)S/Cu_2S$ cell conversion efficiency has increased substantially to a maximum value of 6.29% at an open circuit voltage of 0.64 V. The major improvement in cell performance is in short circuit current which now exceeds 14 mA/cm^2 for open circuit voltages between 0.60 and 0.68 V.

Specific attention has been paid to parameters limiting fill factor in the CdS/Cu_2S cell. The analysis of the mixed sulfide cell is being progressively refined and measurements on open circuit voltage stability, capacitance and the influence of heat treatment are reported.

17. Key Words and Document Analysis. 17a. Descriptors

Photovoltaic Conversion

CdS Solar Cells

Heterojunctions

17b. Identifiers Open-Ended Terms

Solar Energy

17c. COSATI Field/Group

18. Availability Statement	19. Security Class (This Report) UNCLASSIFIED	21. No. of Pages
	20. Security Class (This Page) UNCLASSIFIED	22. Price

USCOMM-DC 14952-P72

Abstract

Maximum power conversion efficiency in actual sunlight for the CdS/Cu_2S cell has reached 8.55% and short circuit currents of 25.0 mA/cm^2 have been measured.

The $(CdZn)S/Cu_2S$ cell conversion efficiency has increased substantially to a maximum value of 6.29% at an open circuit voltage of 0.64 V. The major improvement in cell performance is in short circuit current which now exceeds 14 mA/cm^2 for open circuit voltages between 0.60 and 0.68 V.

Specific attention has been paid to parameters limiting fill factor in the CdS/Cu_2S cell. The analysis of the mixed sulfide cell is being progressively refined and measurements on open circuit voltage stability, capacitance and the influence of heat treatment are reported.

3rd Quarterly Report, January 1, 1977 - March 31, 1977

2. Table of Contents

	Page
Bibliographic Data Sheet	ii
1. Abstract	1
2. Table of Contents	3
List of Illustrations	4
List of Tables	6
3. Summary	8
4. Introduction	9
4.1 Objectives	9
4.2 Approach and Key Methods	9
5. Cell Production and Analysis	11
5.1 Development of CdS/Cu_2S Cells	11
5.2 Development of $(CdZn)S/Cu_2S$ Cells	19
5.3 Electro-Optical and Theoretical Analysis	26
6. References	74
APPENDIX A. List of Research Contributors	75

List of Figures

Figure 1. Sunlight testing of CdS/Cu_2S cell 458A1-4.

Figure 2. X-ray line profiles across pits in the cell surface.

Figure 3. Concentric CdS, ZnS evaporation source.

Figure 4. Etched and unetched surface of a 21% zinc (CdZn)S film.

Figure 5. Sunlight testing of $(CdZn)S/Cu_2S$ cells 418B1 and 418E2.

Figure 6. Total reflectance from various components of the CdS/Cu_2S cell.

Figure 7. Reflectance from cells on brass and zinc substrates.

Figure 8. Cross-section of CdS/Cu_2S cell.

Figure 9. Total reflectance from a high efficiency CdS/Cu_2S cell.

Figure 10. Fill factor as a function of sheet resistance and grid spacing.

Figure 11. Variation of fill factor as a function of short circuit current.

Figure 12. Current-voltage behavior for cell 365D in the high efficiency and excessively heat treated state.

Figure 13. Calculated fill factors as a function of Cu_2S hole concentration.

Figure 14. Current-voltage curves using filtered illumination.

Figure 15. Cu_2S thickness as a function of reaction time in a cuprous chloride solution.

Figure 16. Open circuit voltage for (CdZn)S/Cu_2S cells 10 mA/cm^2 light generated current.

Figure 17. Capacitance as a function of zinc content for (CdZn)S/Cu_2S cells.

Figure 18. The influence of etching on the capacity and short circuit current of (CdZn)S/Cu_2S cells.

Figure 19. Band diagram for CdS/Cu_2S junction.

Figure 20. Dark voltage decay for a (CdZn)S/Cu_2S solar cell.

Figure 21. Dark voltage decay for a CdS/Cu_2S solar cell.

List of Tables

1. Predicted and achieved performance figures for the present cell design.

2. Collimated sunlight test results for cells with all evaporated grid structures and an SiO anti-reflection coating.

3. Composition and resistivity distributions for (CdZn)S films made using the concentric evaporation source.

4. Total reflectivity for substrate 426 after etching.

5. Influence of etching and heat treatment on (CdZn)S/Cu_2S cells, #413.

6. Natural sunlight testing of (CdZn)S/Cu_2S cells.

7. Influence of zinc plating thickness on short circuit current.

8. Short circuit current computed for various material parameters and substrate reflectance.

9. Current losses due to substrate absorbtion.

10. Values used to compute the curves in Figure 13.

11. Cut off filters used generating Figure 14.

12. I-V behavior under cut-off illumination.

13. I-V results for various (CdZn)S/Cu_2S cells.

14. Heat treatment effect in solution reacted (CdZn)S/Cu_2S cells.

15. Apparent energy gaps deduced from spectral response measurement.

16. Trap levels in CdS.

3. Summary

The maximum power conversion efficiency achieved with CdS/Cu_2S cells has been increased to 8.55% in actual sunlight testing. The maximum short circuit current has reached 25.0 mA/cm^2. The cell designed currently being utilized has an all evaporated gold grid of 96% transmission and a single layer of silicon monoxide antireflection coating.

The (CdZn)S/Cu_2S cell conversion efficiency has been increased substantially during the quarter and at an open circuit voltage of 0.64 V an efficiency in actual sunlight of 6.29% has been achieved. At an open circuit voltage of 0.68 V, the efficiency has reached 5.87%. The major cause for the improved conversion efficiencies are higher short circuit currents which have exceeded 14 mA/cm^2 for open circuit voltages between 0.60 and 0.68 V.

The conversion efficiencies being achieved with the CdS/Cu_2S cell are currently limited by fill factor. Whereas analysis indicates that fill factors up to 73% are achievable, the high efficiency cells are only showing fill factors of the order of 67%. Extensive experimental and theoretical analysis of fill factors have been carried out and some progress made towards achieving the theoretical values. Total reflection measurements have been used extensively to more closely quantify the photon economy of the cell and important effects due to substrate reflection identified.

The analysis of the mixed sulfide cell is being progressively refined and measurements on open circuit voltage stability, capacitance, and the influence of heat treatment are reported.

4. Introduction

The program goal is the production of a thin film polycrystalline cell with a 10% power conversion efficiency. Two related heterojunctions are being developed, the CdS/Cu_2S and $(CdZn)S/Cu_2S$. The better developed cell, CdS/Cu_2S, has continued to improve in efficiency and a value of 8.5% has been achieved. A modification of this cell using the mixed cadmium zinc sulfide has also shown substantial improvement, particularly in short circuit currents. The maximum efficiency achieved with this cell has reached 6.29%.

4.1 Objectives

The long term objective of the present program is a low cost thin film polycrystalline cell for terrestrial power generation. The immediate objective is to increase the power conversion efficiency of laboratory cells to more than 10%. Materials and electro optical analyses are conducted in order to quantify the structure and the properties necessary to achieve such efficiency. As higher efficiencies are reached, increasingly sophisticated and precise characterization techniques become necessary and are being developed as part of this program.

4.2 Approach and Key Methods

The basic cell formation procedure continues to be the vapor deposition of a CdS or (CdZn)S layer. The p-type Cu_2S layer is being produced by either solution or solid state reaction with cuprous chloride. The key to the continued improvement in thin film performance is the close coupling of analytical techniques and modeling with the cell production

Quantitative loss analysis for the particular cell design being produced directs the selection of improvement modifications and establishes when specific design limits have been reached.

5.1 Development of CdS/Cu_2S Cells

During this quarter attention has been focused on cells with an all evaporated grid structure and an SiO anti-reflection coating. Actual sunlight testing achieved power conversion efficiencies of 8.5% and short circuit currents of 25.0 mA/cm^2.

Gridding and Anti-Reflection Coating

In the last quarterly report,[1] a new tab and grid structure for the Cu_2S/CdS cell was described. The reason for the cell redesign was that the design limit had been reached for the conventional pressure bonded grid cell. Rothwarf and Barnett[2] have analyzed the losses involved in that design and predicted the performance to be expected from the new cell design.

The major design changes incorporated in the new structure are:

1) Higher optical transmission for the top collection electrode through the use of narrower current collection lines. Fine spacing of the lines to minimize Cu_2S sheet resistance losses was maintained. Both 60 and 80 lines/inch were found acceptable as was expected for the 0.2 μm thickness of Cu_2S employed on these cells

2) An SiO antireflection coating was evaporated onto the Cu_2S to minimize reflection losses at the Cu_2S/air interface. The integrated reflection losses achieved with the best cells are reported in Section 5.3. The SiO appears to act as a getter for oxygen, reducing the copper oxide

surface layer and is porous enough to permit optimizing the Cu_2S by heat treatments after the AR coating is applied.

Several major problems and their solutions were detailed in the last report.[1] During the first production runs on the new cells, several additional problems necessitating process changes arose:

1) The gold lines (12 μ nominal width) used as current collectors are vapor deposited through an aperture mask in contact with the cell. Problems with discontinuous lines developed at these narrow line widths. To prevent excessive line broadening, the gold source must subtend as small an angle as possible at the sample consistent with acceptable evaporation rates. Shadowing of a portion of a line during the evaporation then becomes likely, resulting in discontinuous collector lines. Achievable levels of mask quality did not eliminate this problem and cell yields were low with many cells showing low fill factors due to the additional series resistance.

The problem was cured by using two buss bars deposited perpendicularly to the collector lines in a second evaporation. The lines were located at the 1/3 and 2/3 position along the main grid lines. The redundancy in current flow paths cured the problem with a minor transmission loss of ≃ 1%.

2) A second problem with the narrower lines occurred at the collection tab. The new cell design utilizes a

current collection tab insulated with 12 μm thick epoxy sheet. Using the gold line thickness calculated on the basis of current carrying ability for an ideal planar system, namely 1.5 μm, it was found that the point where the gold lines climb the insulator edge is very prone to failure. This first appears as an anomolously high series resistance and, finally when all lines fail, an open circuit. The combination of the buss bars and a thicker line, 2.5 μm, eliminated this failure mechanism.

3) A post fabrication heat treatment has been found to be necessary for all CdS/Cu_2S cells. The behavior of the evaporated grid cells upon heat treatments has been found to be very different from the previous laminated cell and a new optimization procedure has been developed for these cells. The new procedure is characterized chiefly by its simplicity: after the tab lamination process which requires 1/2 hour at 190°C and one hour at 170°C the cell is treated in 10% H_2/90% Ar for 6-15 hours at 150°C to optimize the Cu_2S. This treatment is repeated as necessary to maintain the J_L value at its maximum.

The evaporated gold grids have removed many of the spurious effects associated with instabilities in the pressure bonded grids during heat treatment and show high stability during long periods of heat treatment.

Test Results

Cell development for a given design is continued until the performance reaches 95% of the design figure. The present design limits and actual sunlight performance are shown in Table 1 and Figure 1. Table 2 gives the performance achieved with other cells in the same series.

Table 1

Predicted and Achieved Performance Figures
for the Present Cell Design

Parameter	Predicted	Achieved (Cell 458A1-4)	
Reflection losses %	5	7	
Grid shading %	4	4	
		Collimated (80.8 mW/cm^2)	Global (91.8 mW/cm^2)
J_{sc} (mA/cm^2 at 100 mW/cm^2)	25.0	25.0	25.1
V_{oc} (V)	0.51	0.51	0.52
FF (%)	73	66.9	66.4
EFF (%)	9.3	8.55	8.57

Table 2

Collimated Sunlight Test Results for Cells with All Evaporated
Grid Structures and an SiO Anti Reflection Coating

Cell	Insolation (mW/cm^2)	V_{oc} (V)	J_{sc} (mA/cm^2)		FF (%)	EFF (%)
442 B1-1	95.8	0.50	23.7	(24.8)*	67.6	8.38
442 B1-2	94.1	0.50	22.9	(24.3)	66.5	8.14
455 B1-1	93.6	0.51	21.6	(23.1)	67.3	7.91
455 B1-2	93.4	0.51	20.3	(21.7)	69.1	7.63
455 B2-1	93.5	0.51	20.3	(21.8)	71.2	7.93
455 B2-2	93.8	0.51	20.4	(21.8)	69.4	7.71
456 A2-3	93.8	0.50	22.0	(23.5)	68.6	8.08
458 A1-4	95.2	0.51	23.8	(25.0)	66.9	8.55

*Current density at 100 mW/cm^2.

Cell 458Al-4
Area 1.26 cm^2

	Collimated	Global
Intensity (mw/cm^2)	80.8	91.8
V_{oc} (V)	0.51	0.52
FF (%)	66.9	66.4
J_{sc} (ma/cm^2)	20.2	23.0
J_{sc} at 100 mw/cm^2	25.0	25.1
Efficiency (%)	8.55	8.57

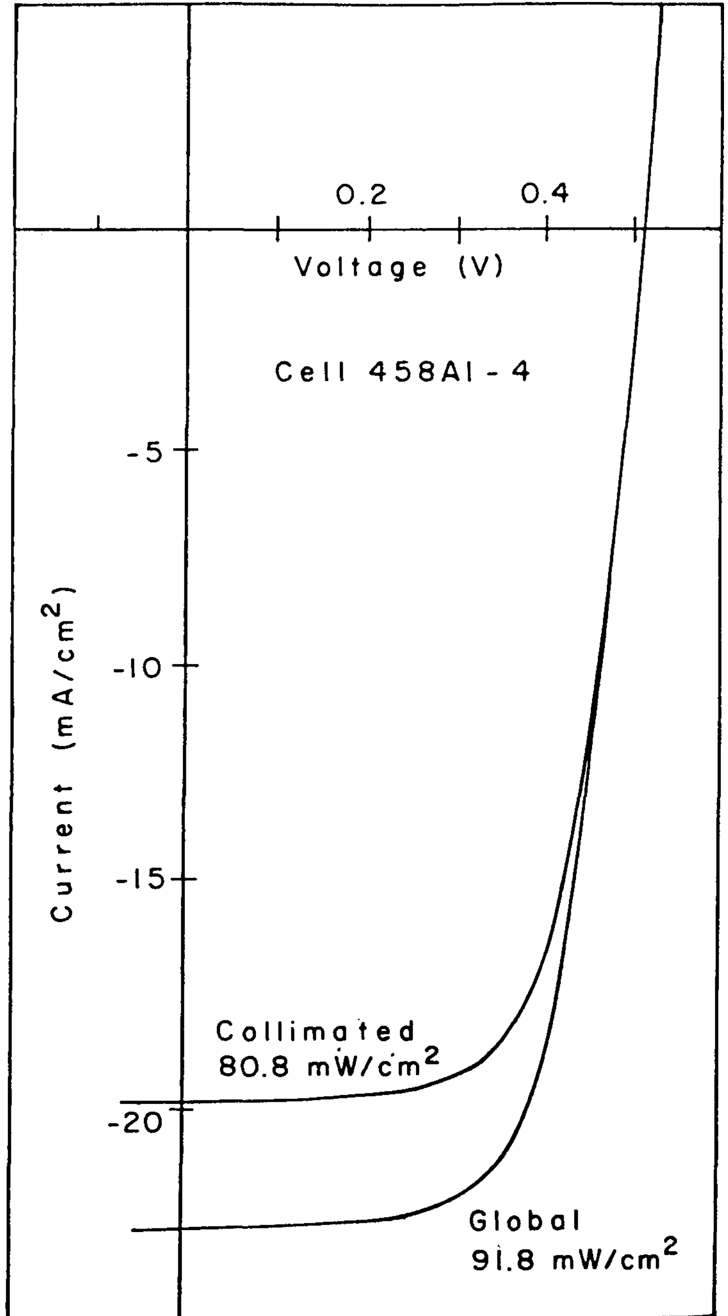

Figure 1. Current-voltage characteristic in actual sunlight for cell 458Al-1.

It is seen that both current and voltage actually exceed the 95% figure and that the fill factor is just preventing the target efficiency (8.8%) being reached. The calculation of achievable current is dependent on the spectrum used and is subject to some uncertainty. The problems and solutions associated with fill factor are discussed below.

Fill Factor and Shunting Problems

It has previously been proposed that the shunting encountered on Cu_2S/CdS cells with evaporated grids was due to contact between the gold grid and the CdS and, in extreme cases, between the gold grid and the substrate. It was further proposed that heat treatments effectively removed the shunt from the cell by creating a blocking contact between the gold and the CdS.

During this reporting period, direct evidence has been obtained showing that CdS is exposed through the nominally continuous layer of Cu_2S for certain cells. Using x-ray emission detection on an SEM the concentration of a given element along a line across the cell surface can be determined. Fig. 2a shows the copper and cadmium line profile on cell 456A1. Examination of the figure shows that the copper concentration falls to zero across the entire width of the pit whereas the cadmium line only drops to zero towards the right hand side of the pit. This drop in Cd arises because the side of the pit obstructs the x-rays and prevents them reaching the detector. In the region where the Cd can be detected, it follows that the drop in Cu counts is a real effect and there is indeed no surface Cu_2S film at the bottom of the pit. The presence of pits does not necessarily mean that the Cu_2S layer is discontinuous as is shown in

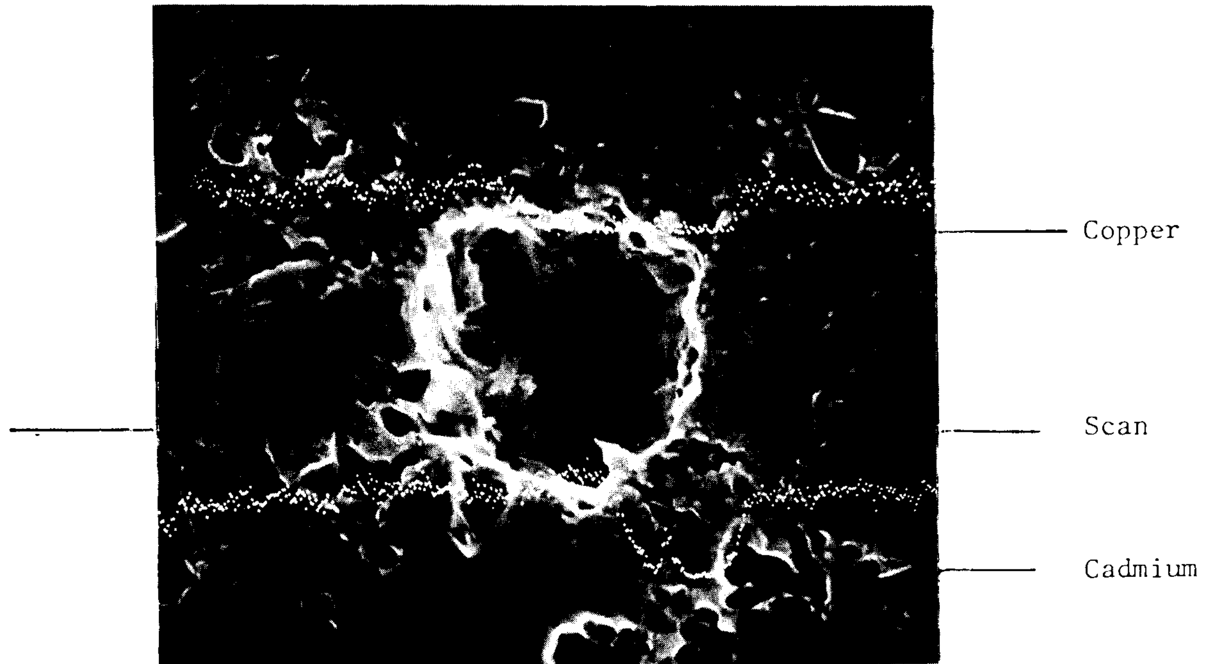

(a)

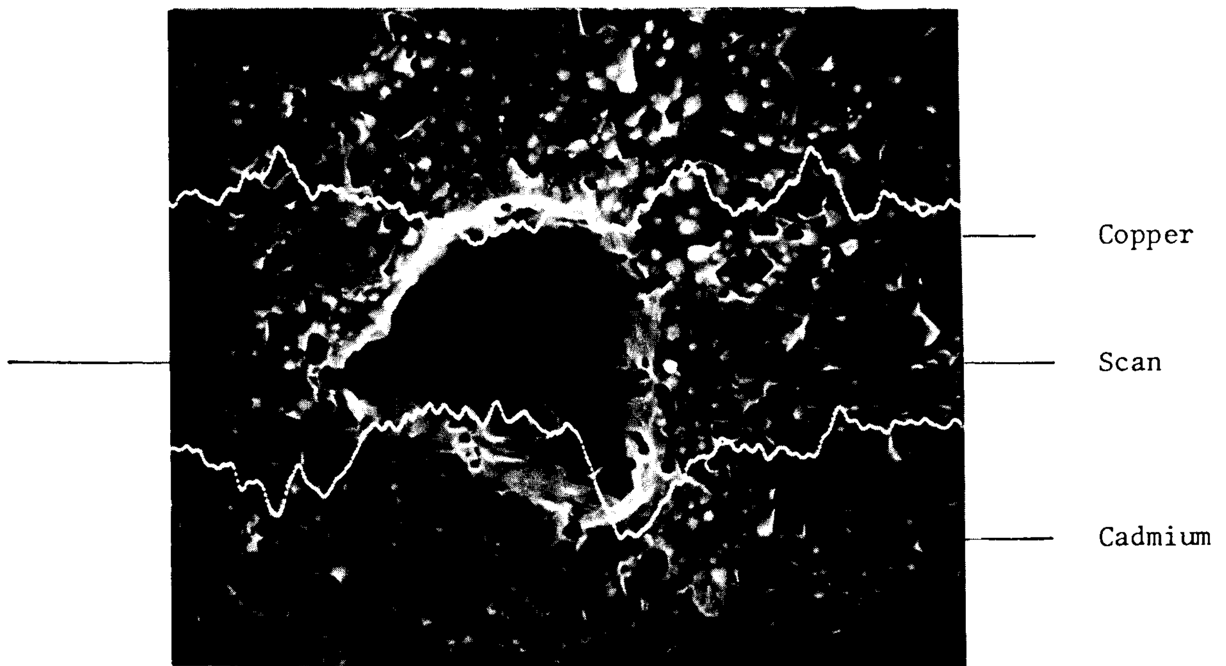

(b)

10 μ

Figure 2. X-ray line profiles across (a) cell 456A1 (b) cell 440B2

Figure 2b for cell 440 B2. In this case the copper profile does not fall to zero even where the Cd signal is very low reflecting the more penetrating nature of the CuKα line compared to the CdL x-ray. The major difference between the two substrates was that the zinc plate was much thinner on the 456 series. This question is further discussed in Section 5.3 in reference to the reflectivity of the metal substrate. The initial conclusion is that grain dropout after Cu_2S formation is more likely on the thinner zinc substrates. Further investigation of the various effects of zinc plate thickness on cell yield and efficiency are in progress.

5.2 Development of (CdZn)S/Cu_2S Cells

A continuous improvement in short circuit current and cell efficiency has been achieved during this quarter. Specific attention has been directed to control of the (CdZn)S deposition and the elucidation of the current controlling mechanisms in the mixed sulfide cells.

Growth of (CdZn)S Films

The two and three-source growth techniques previously reported resulted in fairly uniform films but the films were not easily reproducible and had generally high resistivities. During this quarter a new source was designed and fabricated, and has recently been tested. A cross-section of the source is shown in Figure 3. The zinc composition is primarily controlled by the CdS and ZnS orifice sizes and the resistivity by the source temperature. Two depositions were carried out using this source before the end of March. Zinc composition and electrical resistivity values measured at three positions across a 3" x 3" substrate diagonal are shown in Table 3.

Table 3

Composition and Resistivity Values for Two Mixed Sulfide Substrates Deposited Using the Concentric Source

		% Zinc	Resistivity (Ohm-cm)
Run 489	corner	23.6	142
	center	24.3	248
	corner	23.5	135
Run 490	corner	21.8	23
	center	21.3	82
	corner	22.9	84

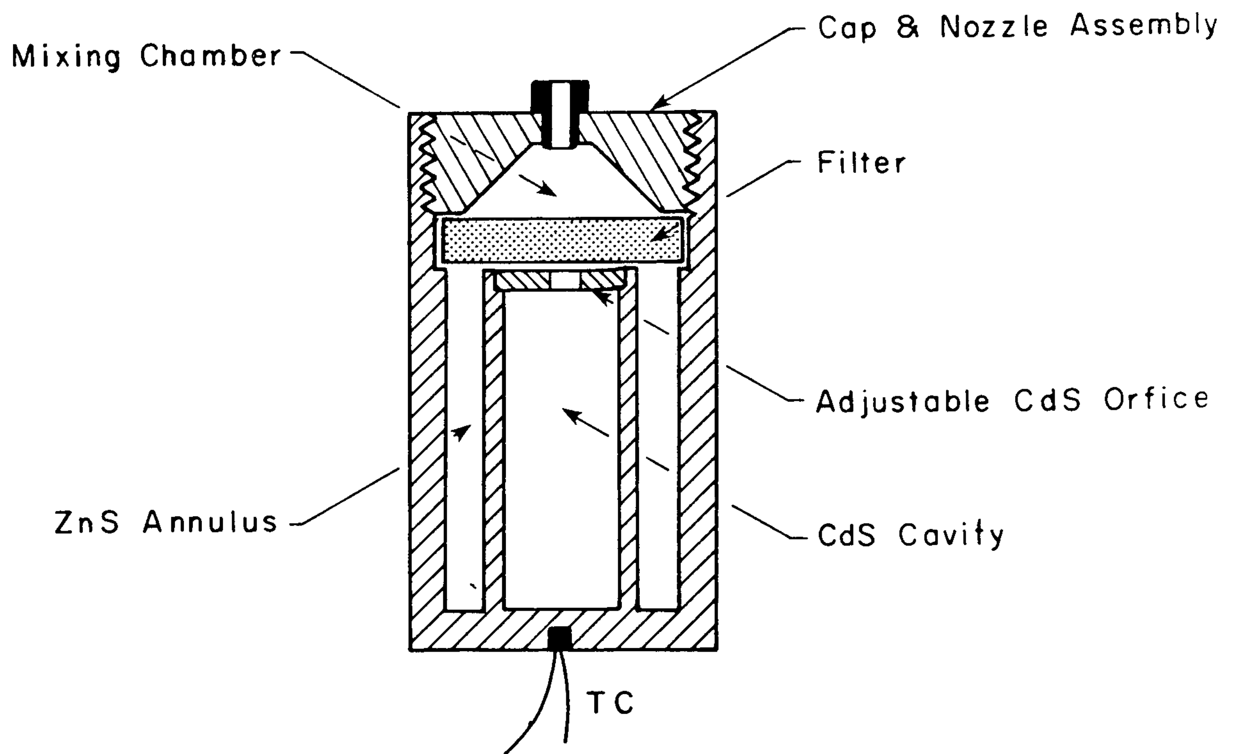

Figure 3. Concentric evaporation source for CdS and ZnS.

This data verifies that a laterally uniform film of ∿ 20 μm thickness can be grown using the new source. Experiments underway will clarify the dependence of film properties on CdS orifice size and source temperature. The present goal is the ability to deposit films in the 10-20% zinc range of resistivities ≤ 20 Ω cm. Depositions made during April 1977 indicate that these goals can be obtained and will be reported in the next progress report.

Etching Behavior of (CdZn)S

The low reflectivity achieved with the conventional CdS cell is due to the textured, light trapping surface produced by a brief HCl etch. Direct S.E.M. observations and reflectivity measurements have been made to confirm that the same effect is achievable with (CdZn)S. Figure 4 shows the unetched and etched surface of (CdZn)S substrate #490 (∿ 21% Zn). It is seen that the light trapping structure is well formed after only 2 seconds etching and further etching only results in opening up more fissures.

Total reflectivity measurements as a function of etching time are given in Table 4 and show that for 2 seconds or longer etching the total reflectivity is down to 7-8% as is the case for CdS.

Table 4

Total Reflectivity as a Function of Etch Time in 55% HCl at 60°C. Substrate 426 $(Cd_{.85}Zn_{.15})S$.

Time	Reflectivity
0	23%
1 sec	12
2	8
3	7

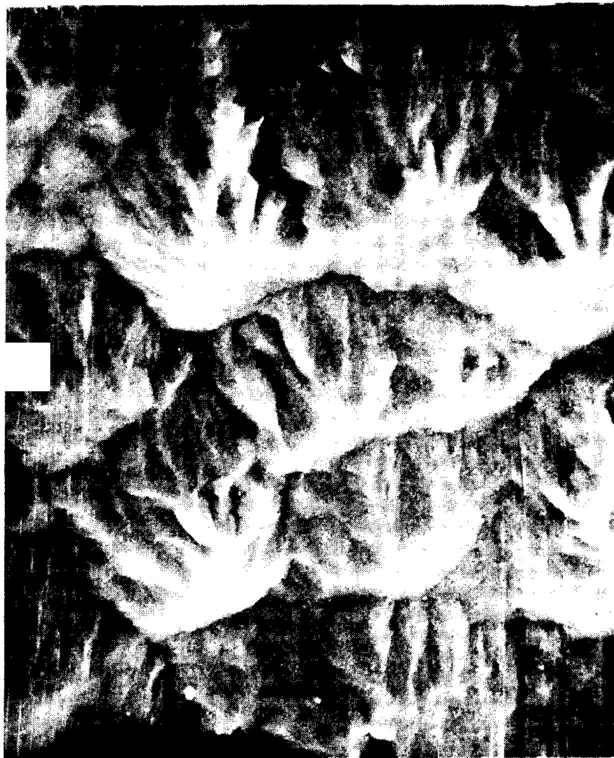

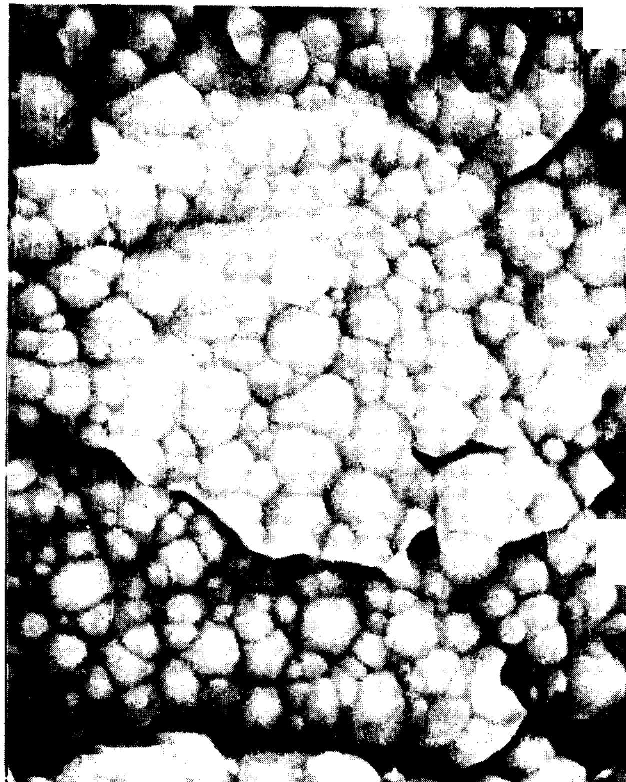

Figure 4. Scanning electron micrographs of the surface of (CdZn)S/Cu_2S cell #490, 21% Zn. (a) As deposited (b) 2 second etch in 55% HCl at 60°C (c) and (d) 4 second etch.

Cell Efficiency and Short Circuit Current Improvement

Early mixed sulfide cells were made using the solid state reaction on unetched substrates. For ease of performing many screening experiments the gridding used was 10 x 60 ℓpi grids pressure bonded to the cell surface. This cell design results in significant current density penalties and accordingly a change to the hybrid grid system was made. In addition, the effects of etching the (CdZn)S and post formation reducing heat treatments were explored. As a consequence, marked improvements in short circuit current density and efficiency were achieved as listed in Tables 5 and 6.

Table 5

Influence of Etching and Heat Treatment on the Properties of $(CdZn)S/Cu_2S$ Cells. Series #413, W-I Simulation

		After Gridding					After 5 Hours H_2/Ar at 170°C			
Cell #	Zn%	Etch*	V_{oc}	J_{sc}	FF	η	V_{oc}	J_{sc}	FF	η
A2	7	0	.61	8.6	67.9	3.57	.61	12.6	65.1	4.95
E2	7	1	.57	9.9	50.2	2.83	.63	14.5	64.5	5.89
E4	5	1	.56	11.4	52.7	3.37	.59	15.3	58.5	5.27

*Etch time (seconds) in 53% HCl at 60°C

Table 6

Natural Sunlight Testing of $(CdZn)S/Cu_2S$ Cells

Cell #	Zn (%)	Insolation (mW/cm^2)	V_{oc} (V)	J_{sc} (mA/cm^2)		FF (%)	EFF (%)
413 E4	5.3	82.8	0.60	13.5	(16.3)*	58.3	5.73
413 E2	7.4	80.9	0.64	12.7	(15.7)	62.3	6.29
418 B1	7.0	83.7	0.68	11.9	(14.2)	61.3	5.87

*Current density at 100 mW/cm^2.

The current-voltage characteristics of cells 418B1 and 413E2 in sunlight are shown in Figure 5.

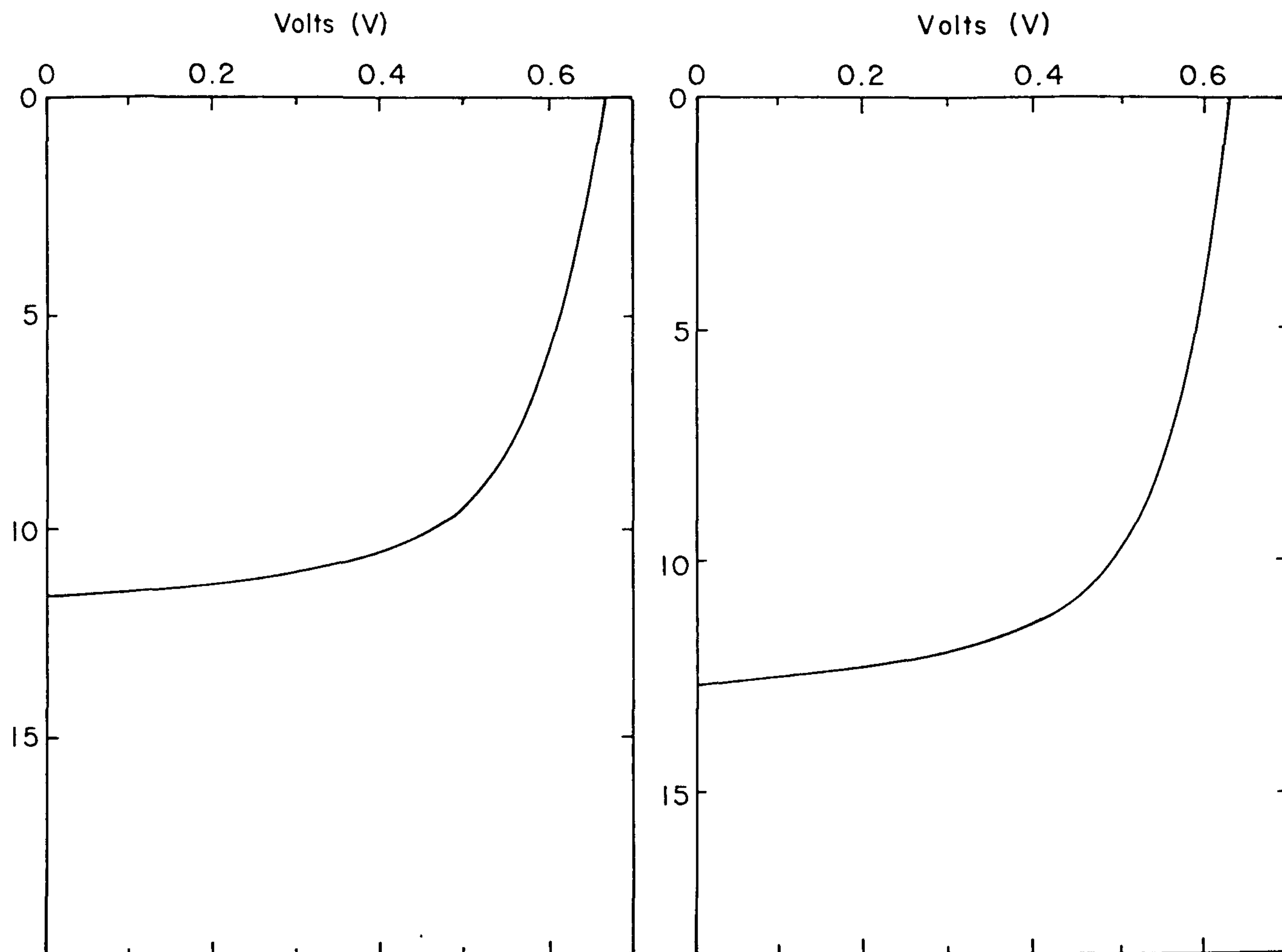

CELL 418B1		CELL 413E2
83.7	INSOLATION (mw/cm^2)	80.9
0.68	V_{oc} (v)	0.64
11.9	J_{sc} (ma/cm^2)	12.7
61.3	FF %	62.3
5.87	EFFICIENCY %	6.29
14.2	J_{sc} (100 mw)	15.7

Figure 5. Collimated sunlight testing of $(CdZn)S/Cu_2S$ cells 418B1 and 413E2.

5.3 Electro-Optical and Theoretical Analysis

Experimental and theoretical analyses have been carried out on cell reflectivity, fill factor, Cu_2S formation, and capacitance for CdS/Cu_2S cells and on various aspects of the (CdZn)S/Cu_2S cells. Current-voltage instabilities in both the light and dark have been studied for both types of cells.

Measurements of total reflectivity have been made previously in the cell improvement program and during this quarter the key role played by reflection from the metallic substrate has been identified.

The efficiency of the present generation of cells is being adversely affected by fill factor and a major effort has been made to identify the controlling parameters.

Observation of cell capacitance have been used to infer the presence of deep levels in the CdS and to explain the influence of heat treatment temperature on copper compensation. Some aspects of the rate limiting mechanisms for the Cu_2S formation process are also reviewed.

A number of experiments have been conducted on the (CdZn)S/Cu_2S cells to further identify the similarities with and differences to the CdS/Cu_2S cells and in both types of cells the time dependent current-voltage characteristics have been further analyzed.

Substrate Reflection Effects

The accurate photon accounting in active CdS/Cu_2S cells has been instrumental in the cell improvements achieved to date. Total reflectance

measurements as a function of wavelength are conducted in a Beckman DK-2A spectrophotometer with a Gier-Dunkle integrating sphere. While exploring the effects on cell yield of changing the thickness of the zinc plating on the copper substrate, it was noted that cell short circuit currents were also varying. A specific set of measurements are given in Table 7.

Table 7

Influence of Zinc Plating Thickness on Short Circuit Current, W-I Simulation

Substrate	Zinc Thickness (μm)	J_{sc} (mA/cm^2)
443	0.75	16.5
444	1.5	14.9
445	3.0	14.2
446	6.0	13.9

It is known that the zinc alloys with the copper to produce a brass during heat treatment and one mechanism whereby the specific state of the substrate could influence J_{sc} would be by changes in the reflection of light that had passed through the CdS. Accordingly, a series of measurements were made of the reflectivity of various layers that make up the cell. Figure 6 shows the reflectance spectra of several cell components for substrate 472 C1 before any heat treatment.

Curve

1 Electrocleaned copper sheet

2 Zinc plated copper sheet

3 Cadmium sulfide on Zn/Cu

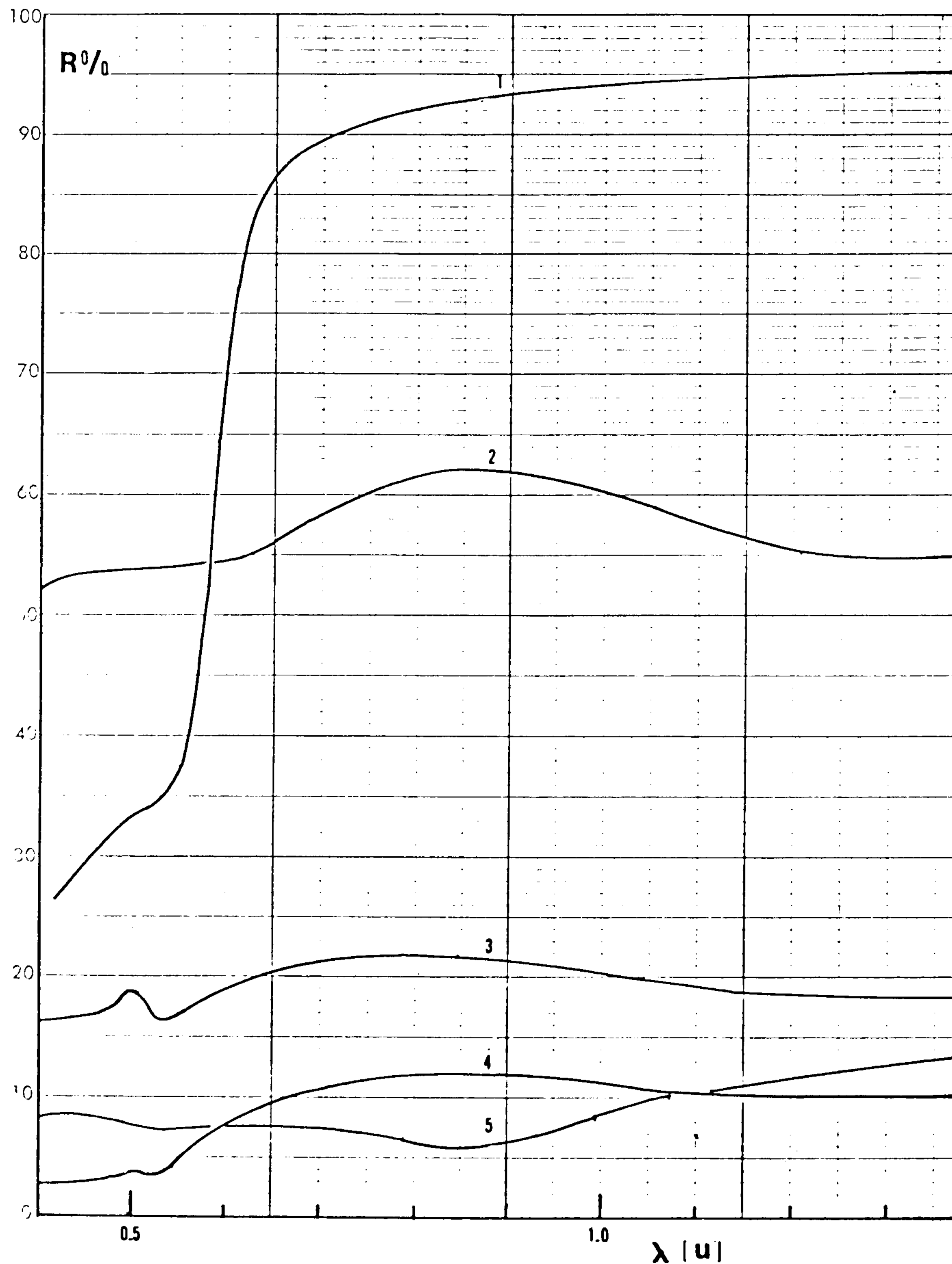

Figure 6. Reflectance from various layers of a CdS/Cu_2S cell. 1. Electro-cleaned copper sheet. 2. Zinc plated copper sheet. 3. CdS layer as deposited on Zn/Cu. 4. CdS layer etched for 2 seconds in HCl. 5. Cu_2S on etched CdS.

4 Cadmium sulfide etched for 2 seconds on Zn/Cu

5 Cu_2S on etched CdS/Zn/Cu

From the curves it can be seen that copper is much more reflecting than zinc above 600 nm, a point that will be returned to later. The marked reduction in CdS reflectance produced by etching and the charges produced by the Cu_2S layer are also seen in Figure 6.

In order to test the hypothesis that the reflectivity of the substrate was influencing short circuit current, cells were made on copper plated with 3.0 and 0.4 μm of zinc, 471C and 471D respectively.

Pieces of the substrates were given heat treatments similarly to those given cells and reflectivity then measured. Figure 7 reveals the marked extra reflectance at long wavelengths for the 0.4 μm Zn which alloyed to α-brass. The surface layer of the 3.0 μm Zn is still unalloyed and gives the low reflectance of zinc at wavelengths above 600 nm. The figure also shows that the extra light reflected by the brass substrate is not absorbed by the CdS layer and is therefore available for carrier generation in the Cu_2S layer. Measurements on the cells produced from these substrates did in fact show that the 471D series had short circuit currents 13% higher than the 471 C series. A photon flux analysis is presented below which shows that these results are consistent with the model that extra reflectance at the brass substrate is giving the higher current.

The photon flux in the Cu_2S layer is given by the following expression (Figure 8):

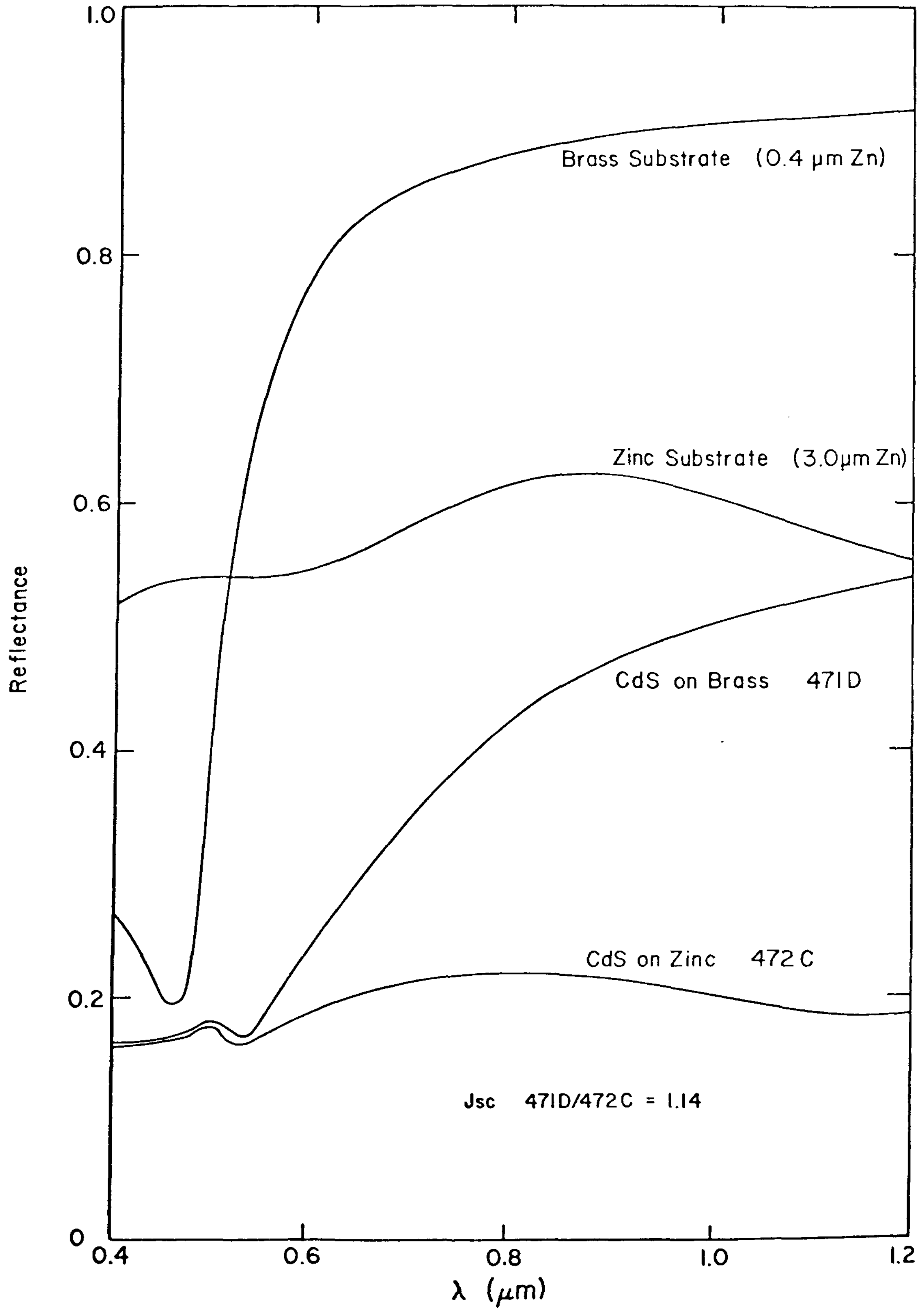

Figure 7. Reflectance from metallic substrates with zinc or brass surfaces and from completed cells on these substrates.

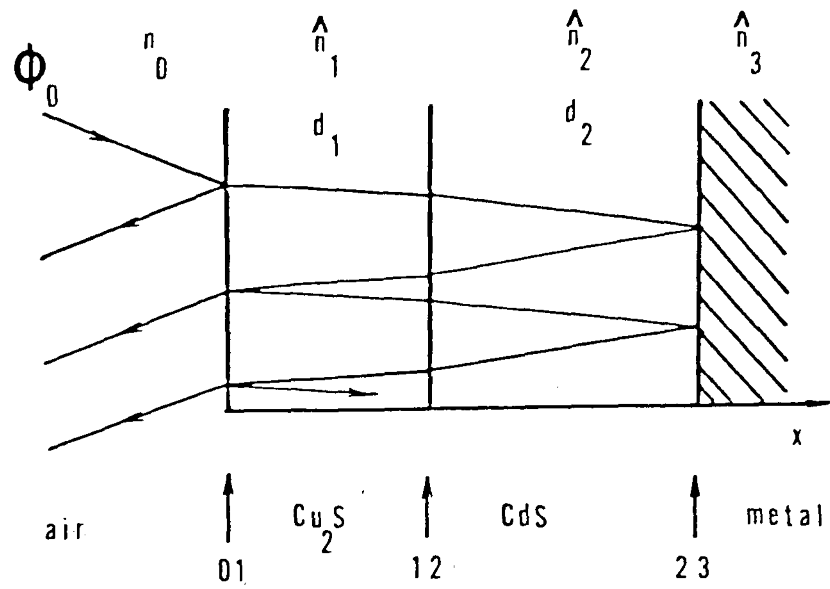

Figure 8. Identification of the layers in a CdS/Cu_2S cell.

$$\phi(x,\lambda) = \Phi_0(\lambda)\ T_{01}\ \frac{[e^{-\alpha_1 x} - R_{23}\ e^{-(\alpha_1 d_1 + 2\alpha_2 d_2)} e^{-\alpha_1 (d_1 - x)}]}{1 - R_{10} R_{23}\ e^{-2(\alpha_1 d_1 + \alpha_2 d_2)}}$$

where:

$\Phi_0\ (\lambda)$: Incident photon flux

T_{01}: Transmittance of the air - Cu_2S interface

R_{ij}: Reflectance at the boundary separating media i and j

α_i: Absorption coefficient of medium i

d_i: Thickness of medium i

The above expression assumes incoherent specular reflections at all interfaces and reflection at the Cu_2S:CdS interface, ≃ 2%, has been ignored.

The photon flux given by the above equation has been used to calculate the light generated current, neglecting multiple reflection between boundaries 01 and 23. The maximum effect on cell current due to absorption at the metal substrate has been calculated assumimg zero and 100% reflectance (R_{23} = 0 or 1)

$$(\Delta J_L/J_L)_{max} = \frac{J_L\ (R_{23} = 1) - J_L\ (R_{23} = 0)}{J_L\ (R_{23} = 1)}$$

Table 8 shows $(\Delta J_L/J_L)_{max}$ for selected values of d_1 and L_1 (minority carrier and diffusion length in Cu_2S). The real loss for $0 < R_{23} < 1$ can be calculated as: $\Delta J_L/J_L = (1 - R_{23})(\Delta J_L/J_L)_{max}$.

Table 8

Achievable Short Circuit Currents for 0 and 100% Reflection at the Metal Substrate for Various Cu_2S Thicknesses, d_1, and Diffusion Distances, L_1[3]

d_1 (μm)	L_1 (μm)	J_L (R_{23} = 0) (mA cm^{-2})	J_L (R_{23} = 1) (mA cm^{-2})	$(\Delta J/J)_{max}$
0.1	0.3	13.92	18.98	0.27
0.1	1.0	14.45	19.68	0.27
0.15	0.3	16.08	20.90	0.23
0.15	1.0	17.51	22.65	0.23
0.30	1.0	22.04	25.73	0.14

The experimental measurements of reflectivity from the CdS layer (Figure 7) can be used to estimate R_{23}. It is not known whether the reflection is specular or diffuse and accordingly an estimate of the extent of light trapping in the CdS cannot be made and this introduces some uncertainty into R_{23}. Taking the extreme cases, completely specular and completely diffuse reflection, and using a Cu_2S thickness and diffusion distance appropriate for un heat treated cells (0.1 and 0.15 μm) the following current losses due to substrate absorbtion are computed.

Table 9

Current Losses Due to Substrate Absorbtion

Substrate	Specular	Diffuse
Brass	16%	6%
Zinc	20%	18%

These results, corresponding to current ratios of 1.14 and 1.15 agree, closely with the experimental measurements on the 471, 472 series of cells. It is of course most likely that the actual reflectance is only partially diffuse.

A typical reflectance spectrum from an SiO coated, high efficiency cell (442 B1-2) can be seen in Figure 9. The low reflectance at $\lambda \simeq 0.5\ \mu$ is due to the SiO layer; and surface texturing and the SiO keep the reflectance below 10% up to 900 nm. The high reflectance above 1100 nm is typical of a high efficiency cell. It can be attributed to a combination of near stoichiometric Cu_2S (no free-carrier absorption) and high R_{23} (due to alloying of zinc with the copper substrate). With the zinc plating thickness normally used, it is only observed after extensive H_2/Argon heat treatment at 150°C when complete alloying to brass has occurred. If the cell is left exposed to the air, the reflection decreases at long wavelengths as the Cu_2S stoichiometry declines and free carrier absorption increases.

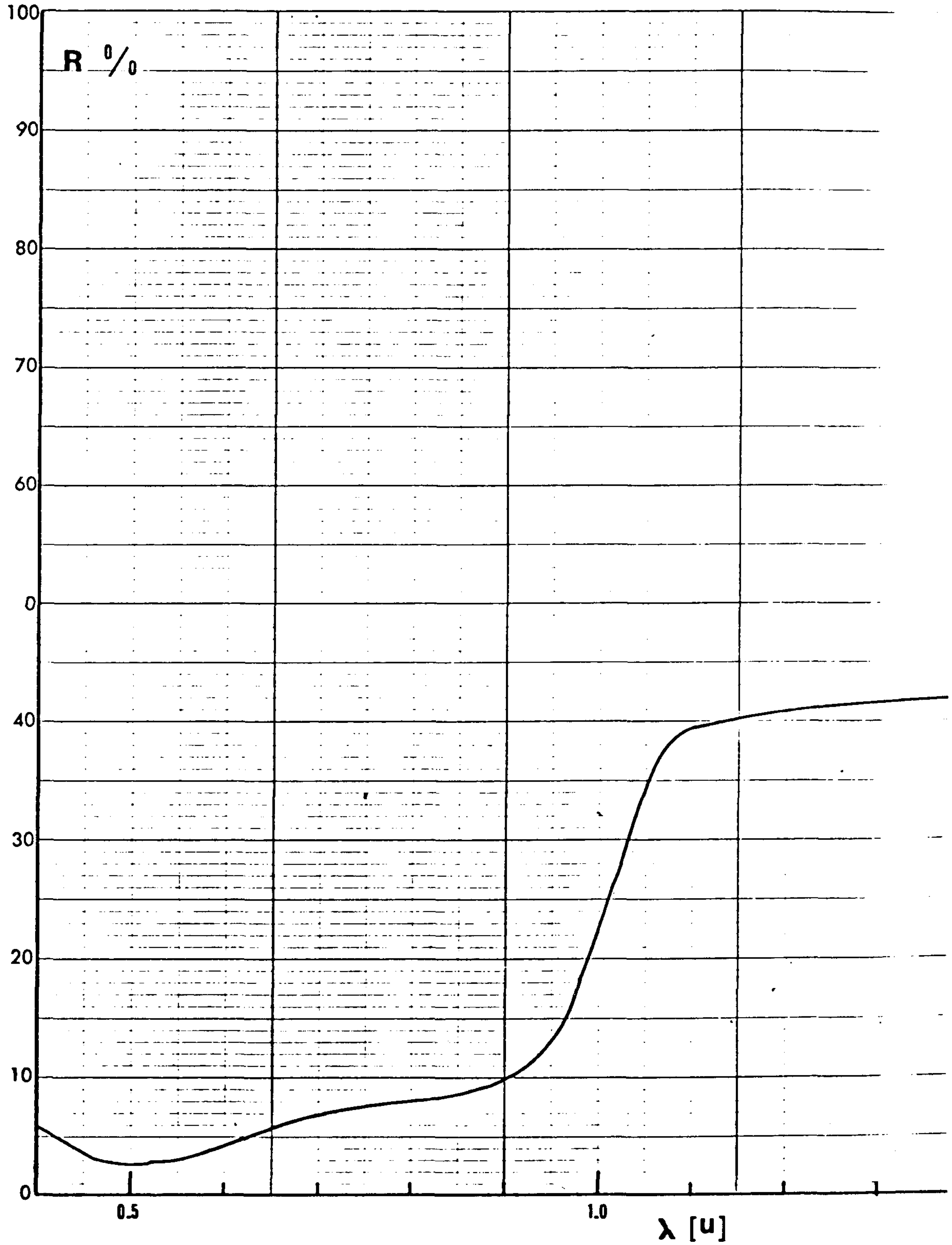

Figure 9. Total reflectance from cell 442B1-2, power conversion efficiency 8.14%.

Fill Factor

Considerable effort in this quarter was devoted to theoretical and experimental studies of the fill factor of the cell. Of the three major cell parameters, short circuit current, open circuit voltage, and fill factor, it is the fill factor which differs most greatly from its theoretically expected value, in high efficiency cells. A thorough theoretical analysis of the factors which can affect the fill factor of a cell was given in the July-September 1976 quarterly report.[4] The factors indicated there which can significantly reduce the fill factor were:

a) Series resistance

b) Variation of j_L with voltage

c) Shunt resistance

The studies undertaken involve studying the current voltage (I-V) relation of the cells after various heat treatments with various types of illumination. The fill factors obtained were analyzed in terms of the loss factors listed above.

a) Series Resistance - Using the linearized expression for fill factor loss and neglecting the other loss mechanisms, the series resistance dependence of the fill factor is given by

$$FF = FF_0 - \frac{j_{sc} R_s AC}{V_{oc}} \quad (1)$$

where FF_0 is the ideal fill factor for a given V_{oc}, j_{sc} is the short circuit current density, A the area of the cell, V_{oc} the open circuit voltage, and the factor C is dependent on V_{oc}. For $V_{oc} \simeq .5$, $FF_0 = .8$ and C = 0.9. For our cells the series resistance is given by

$$R_s A = \frac{\rho}{d} \frac{S^2}{K}; \quad \begin{array}{l} K = 12 \text{ parallel line grid} \\ K \simeq 32 \text{ square grid} \end{array}$$

where ρ is the resistivity of the Cu_2S layer, d the thickness of this layer and S the spacing between grid lines.

The cells studied during this quarter were of varied design, consisting of evaporated parallel line grids with 40, 60 and 80 lines per inch, preformed grids with 60 x 10 lines per inch, and combined evaporated and preformed with 40 x 40 lines per inch. The equivalent thickness of the Cu_2S layer was varied by using dip times of 6, 12, and 16 seconds. A further modification was found to be beneficial in the evaporated line grids, namely cross bars to prevent severe series resistance problems when one or more of the grid lines were either discontinuous or too thin in places.

As reported previously, heat treatment of the cell in a H_2-Ar ambient can increase the resistivity of the Cu_2S dramatically, i.e., by a factor of 10 or more. Subsequent exposure to air reduces the resistivity. These changes are related to the reduction and oxidation of a few monolayers of Cu_2O on the surface of the Cu_2S, which can change the Cu vacancy density and hence the hole density in the very thin Cu_2S layer by

orders of magnitude. The changes seen in resistivity are accompanied by changes in the observed short circuit current in cells; the higher the resistivity the higher the value of j_{sc} in general. From Eq. (1) we expect that as j_{sc} increases FF will fall since in general a high j_{sc} requires high stoichiometry Cu_2S and hence a high ρ value. Eq. (2) indicates how R_s can be minimized while keeping ρ and hence j_{sc} high; larger d values, smaller S values (more lines per inches) or square grids can be used (previous analysis has indicated that parallel line grid gives optimal efficiency).

In Fig.10 we illustrate the expected variation in fill factor as a function of R_sA and j_{sc}, with the corresponding ρ/d values for parallel grids of 60 and 80 ℓpi. In general, as a cell goes through the heat treatment cycle the higher R_sA and j_{sc} values occur together.

To determine whether Eq. (1) adequately describes the fill factor of the cell, j_{sc} was varied by changing the intensity of the incident light and the fill factors obtained from the I-V curve at each intensity. The results are plotted as $\Delta FF = FF_Q$ - (FF) exp. versus C j_{sc}/V_{oc}. The slope should give R_sA while a non zero intercept would indicate that factors other than series resistance were important. Fig. 11 illustrates the results on two evaporated 60 ℓpi grid cells before cross bars were evaporated. The A cell had been dipped for 6 sec. and had a Cu_2S equivalent thickness of ∿ 1860 Å, while the B cell had a 12 sec. dip and an equivalent thickness of ∿ 3170 Å. They had identical heat treatments. Two factors are immediately revealed by Fig.11. First the large intercepts indicate that Eq. (1) doesn't contain all the important terms. Second, the differences in slopes

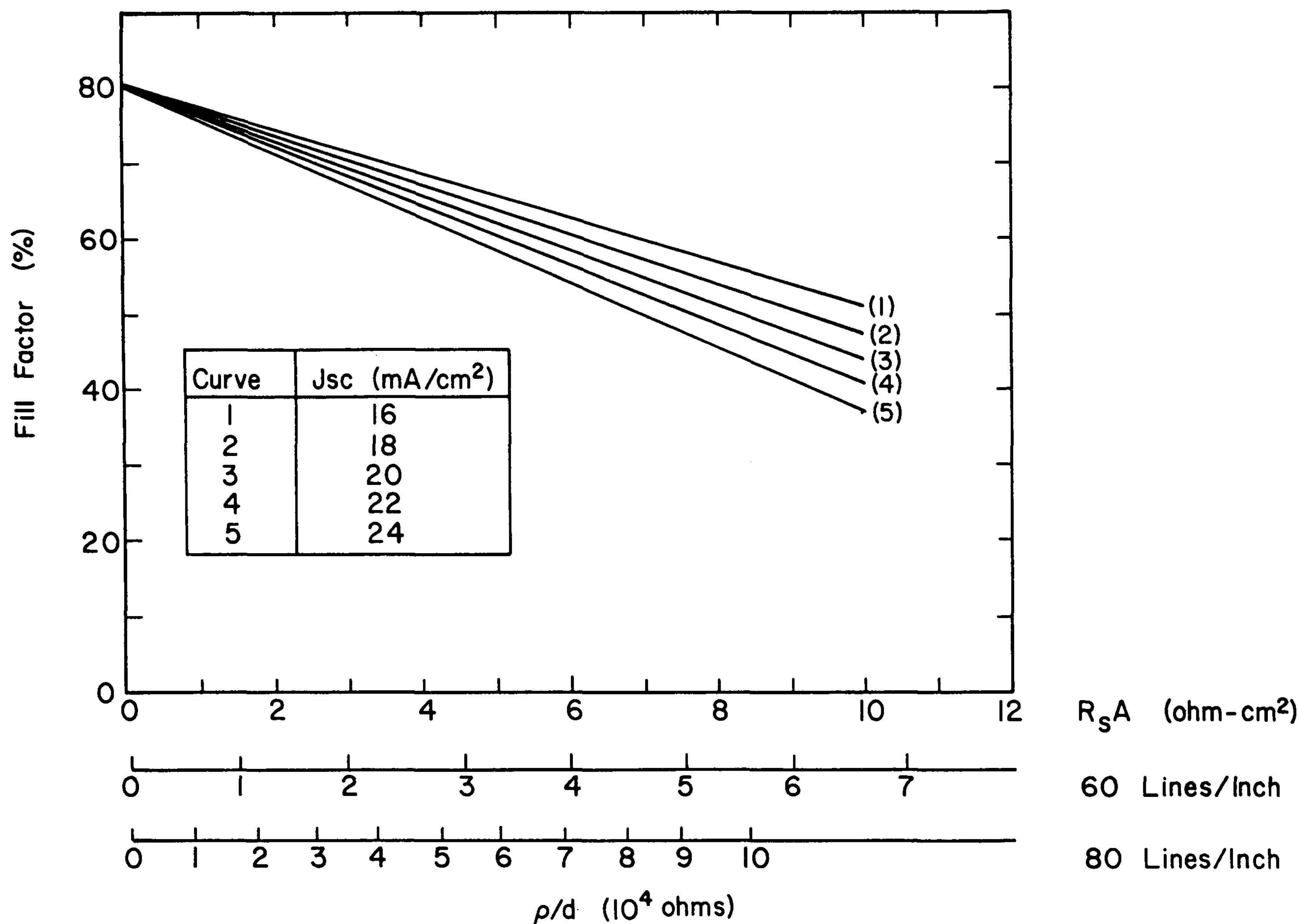

Figure 10. Calculated fill factor using linear theory as a function of $R_s A$ and ρ/d for 60 and 80 parallel line per inch grids.

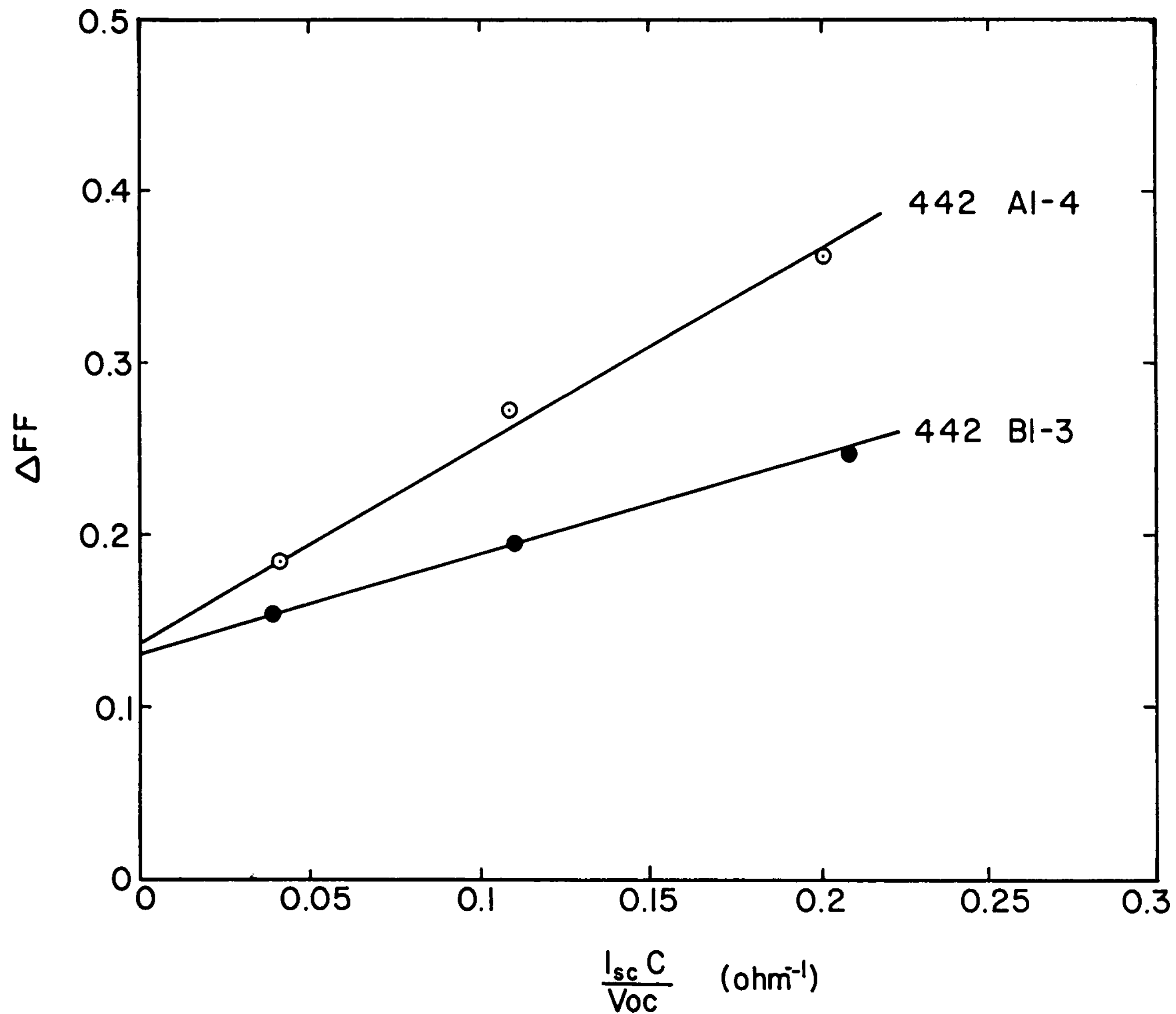

Figure 11. Experimental plot of $\Delta FF = FF_0 - FF_{exp}$ as function of short circuit current, illustrating high intercept values $(\Delta(FF)_0)$.

indicate a significant difference in series resistance between the two cells. From the slopes we obtain $(R_sA)_A = 1.43\ \Omega\text{-cm}^2$ and $(R_sA)_B = 0.80\ \Omega\text{-cm}^2$. Using Eq. (2) we have $(\rho/d)_A = 9.6 \times 10^3\ \Omega$, $(\rho/d)_B = 5.36 \times 10^3\ \Omega$. Using the equivalent thicknesses of the layers gives $\rho_A = 1.78 \times 10^{-1}\ \Omega$ cm and $\rho_B = 1.70 \times 10^{-1}\ \Omega\text{-cm}$. This indicates that the resistivity of the two cells is indeed the same, and that in the determination of the series resistance of the cell it is the equivalent thickness of the Cu_2S layer which enters in Eq. (2).

The intercepts $\Delta(FF)_{0_B} = .13$ are considerably higher than values of $\Delta(FF)_0 \simeq .06$ which had been obtained by this technique previously, with laminated grid cells. Laminated cells from this same substrate were tested in their high resistance state and gave $\Delta(FF)_0$ values of 0.17 and 0.15 with ρ values of $2.9 \times 10^{-1}\ \Omega\text{-cm}$ and $1.74 \times 10^{-1}\ \Omega\text{-cm}$. In this state the laminated cells exhibited a substantial voltage dependence of j_L in reverse bias at high intensities ($\sim$ 5 times AM1). From this behavior it is apparent that Eq. (1) does not give an adequate description of all phenomena observed.

In order to analyze the I-V behavior in more detail, the current voltage expression

$$I = I_0 \{\exp\left(\frac{q\ (V - IR_s)}{k_T}\right) - 1\} - I_L \tag{3}$$

was rewritten as

$$V = I_L R_s f + V_{oc} + \frac{kT}{q} \ln \left(1 + f + \frac{I_0}{I_L}\right) \tag{4}$$

where $f = I/I_L$. Eq. (4) can be solved for the voltage V at which any given value of f occurs. The value of $f = -1$ is reached for $V = V_s = -I_L R_s$. We can also determine the value of f at V = o as a function of $R_s A$. Since f (V = 0) = I_{sc}/I_L it is a measure of how much variation in j_L with voltage is occurring in reverse bias. Based on Eq. (4) with V_{oc} = .5 and j_L = .02 A/cm^2, a value of f(V = o) = -.99 would require $R_s A$ = 19.2 Ω-cm, implies ρ/d values ∿ 1.3 x 10^5 Ω, which are higher than any yet observed either from van der Pauw studies or from fill factor analysis. Yet f(V = o) values on the order of ∿ .9 or less are seen, and saturation of the current at voltages of ∿ -.3 V are not uncommon immediately after H_2-Ar heat treatments. Such large V_s values would, from Eqs. (3) and (4), imply values of ∿ 15 Ω-cm^2 for j_L = .02 Amp/cm^2.

If such large $R_s A$ values are unreasonable based on direct evidence (they would also imply other changes which we will discuss shortly), then what causes small values of f(o) and large V_s values, particularly at high intensities? One can calculate the voltage drop between the grid lines and the mid-point between them due to the short circuit current and obtain the result

$$\Delta V = j_{sc} \frac{\rho S^2}{16d} = 0.75\ j_{sc}\ R_s A = 0.75\ V_s \qquad (5)$$

This voltage drop forward biases that region of the diode between Cu_2S and CdS. For a high resistance cell $R_s A$ = 2 - 3 Ω-cm^2, with j_{sc} = .02 A/cm^2, ΔV = .03 - .05 V. For j_{sc} = 0.1 A/cm^2 (Fresnel lens concentration), ΔV = 0.15 - .23 V. From Eq. (4) such forward biases would not lower f substantially. (For an ideal diode with $R_s A$ = 2 - 3 Ω-cm^2, f at V_{mp} ≃

.4 V is - .93). Hence, another effect is present, that causes f to vary intrinsically with voltage and is accentuated by the effect indicated by Eq. (5).

b) Variation of j_L with Voltage

We have previously derived a relation for j_L as a function of the junction field

$$j_L = j_{L0} \frac{\mu_2 F_2}{S_I + \mu_2 F_2} \qquad (6)$$

The possible variation of F_2 with voltage, CdS resistivity and light was treated in detail in ref. 4. However, the variation of F_2 and j_L with Cu_2S stoichiometry was not treated. In general, we have assumed that the hole density in Cu_2S greatly exceeds the electron density in CdS. Under these circumstances the diffusion voltage is dropped almost entirely in the CdS and the extent of the space charge region in Cu_2S is on the order of 10 Å. If the stoichiometry of the Cu_2S becomes such that appreciable band bending in Cu_2S occurs over a region of several hundred Å, j_{L0} will depend on voltage through the electric field enhanced diffusion length, since much of the carrier generation would take place in a region of high field. In addition, the open circuit voltage would be lower due to both the band bending and the rising of the Fermi level into the gap of the Cu_2S. The field F_2 and its voltage dependence would also be changed under these circumstances.

The diffusion voltage V_D at zero applied bias is given by

$$V_D = V_{Dn} + V_{Dp} = E_{g1} - \Delta\chi - \delta_1 - \delta_2 \qquad (7)$$

where E_{g_1} is the Cu_2S energy gap, $\Delta\chi$ the difference in electron affinity between Cu_2S and CdS and δ_1 the position of the Fermi level in Cu_2S relative to the valence band. The values of V_{Dn} and V_{Dp} and the apportioning of the applied voltage between Cu_2S and CdS is given by

$$\frac{V_{Dn} - V_n}{V_{Dp} - V_p} = \frac{N_A \varepsilon_p}{N_D \varepsilon_n} = r; \; V = V_n + V_p \tag{8}$$

where ε_p and ε_n are the dielectric constants of Cu_2S and CdS (each is $\sim$ 10), and N_A the acceptor density in Cu_2S and N_D the donor density in CdS.

The width of the space charge region in Cu_2S is given by

$$w_1 \; (V) = \left[\frac{2\varepsilon_p \varepsilon_0 \; (V_{Dp} - V_p)}{qN_A} \right]^{\frac{1}{2}} = \left[\frac{2\varepsilon_p \varepsilon_0}{qN_A} \; \frac{(V_D - V)}{r + 1} \right]^{\frac{1}{2}} \tag{9}$$

In reverse bias w_1 will increase, and if N_A is low enough so that w_1 is an appreciable fraction of the thickness of the Cu_2S the changes in w_1 with voltage may be sufficient to account for part of the voltage dependence of j in reverse bias, by changes in j_{LO}.

In addition the expression for F_2 is given in the constant space charge approximation by

$$F_2 = \left[\frac{2qN_D}{\varepsilon\varepsilon_0} \; \frac{r}{r + 1} \; (V_D - V) \right]^{\frac{1}{2}} \tag{10}$$

In our usual assumption r >> 1 (r $\sim$ 100); for lower r values, $\mu_2 F_2$ will become smaller in relation to S_I (assuming it remains constant) and hence its voltage variation more significant.

Under the same assumptions the expression for V_{oc} is given by

$$V_{oc} = \frac{\phi_0}{q} - \frac{kT}{q} \ln \frac{qNc_2S_I}{j_I\ (V_{oc})} + \frac{1}{r} \left(\delta_2 - \frac{kT}{q} \ln \frac{qNc_2S_I}{j_L\ (V_{oc})}\right) \qquad (11)$$

where ϕ_0 is given by

$$\phi_0 = qV_D + \delta_2 = E_{g_1} - \Delta\chi - \delta_1 \qquad (12)$$

The first term in Eq. (11) is the usual expression for V_{oc} ($r >> 1$) and the second represents the correction term due to finite r values.

For a specific example we have evaluated Eq. (11) with $N_A = 2 \times 10^{17}/cm^3$ and $N_D = 6 \times 10^{16}/cm^3$. The result is $V_{oc} = 0.3$ V with, 0.1 V drop coming from the shift in δ_1 and $\sim$ .12 V coming from the second term in Eq. (11). In Figure 12, we show two I-V curves for cell 365D. The dashed curve is for the cell in its high efficiency state $R_sA \simeq 1\ \Omega\text{-cm}^2$ with, $V_{oc} \simeq .5$ V FF $\simeq .65$ and $j_L \simeq 19$ mA/cm^2. The solid curve is the I-V immediately after 15 hr. H_2-Ar at 170°C, with $V_{oc} \simeq .41$, FF -, $j_L\ (V_s) =$ 19 mA/cm^2, $j_{sc} = 14.4$ mA/cm^2. With storage or mild heating in air the solid curve relaxes to the dashed curve. One can cycle back and forth between the dashed and solid curves obtaining a variety of intermediate curves with V_{oc} values between the extremes shown in Fig.12 and with various V_s and f(0) values.

Using Eqs. (3), (6), and (10) with

$$I_0 = Aj_0 = AqN_{c_2}\ S_I \exp - \phi_0/kT \qquad (13)$$

and the values in Table 10 computer calculation of fill factor yield the results shown in Fig. 13. These results combine the R_s effects and part of

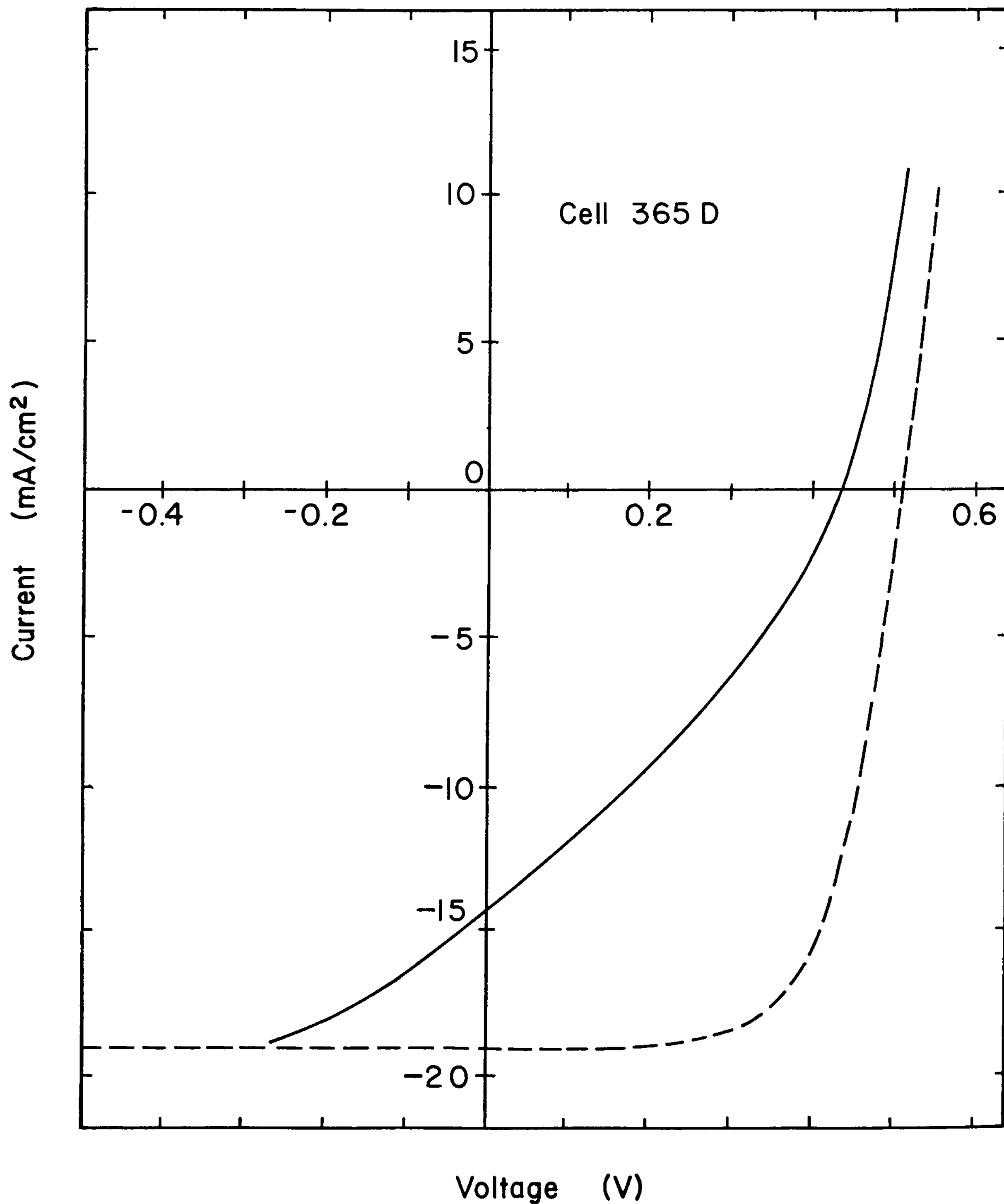

Figure 12. Current voltage curves at AM1 simulation, showing the effects of H_2-Ar heat treatment on the cell characteristics. Continuous curve is before H_2-Ar heat treatment.

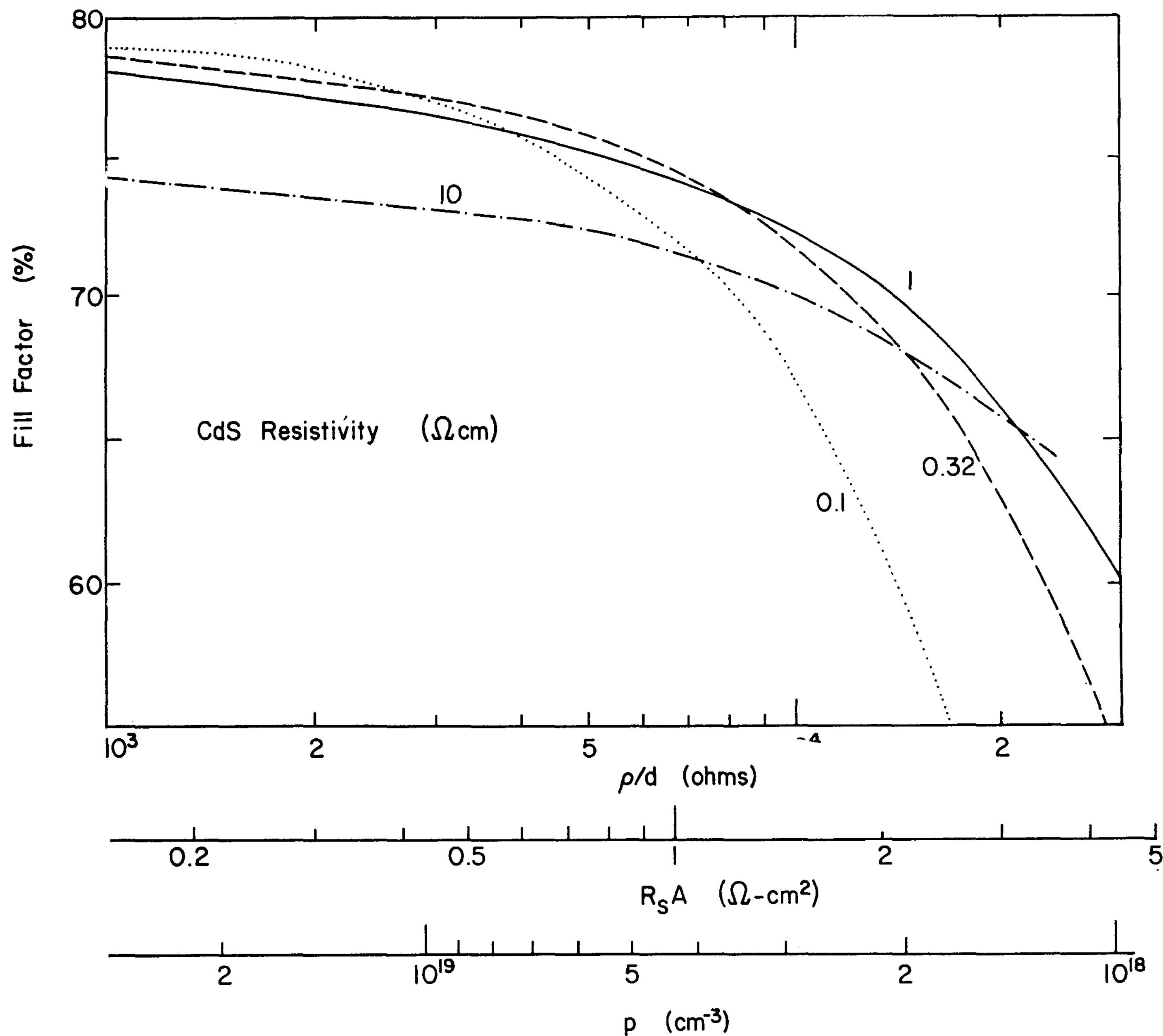

Figure 13. Calculated fill factor as a function of Cu_2S hole concentration and CdS resistivity using parameters of Table 1.

Table 10

Values Used in Numerical Computation for Fig. 13

$N_{v_1} = 4.6 \times 10^{19}$ cm^{-3}

$N_{c_2} = 2.3 \times 10^{18}$ cm^{-3}

$\varepsilon_p = \varepsilon_n = 10$

$\Delta\chi = .2$ eV

$N_{D_2} = n_2$

$N_{A_1} = p_1$

$T = 28°C$

$\mu_1 = 10$ cm^2/V-sec; $\mu_2 = 100$ cm^2/V-sec

$S_I = 10^6$ cm/sec

60 line per inch grid

$J_{L_0} = 20$ ma/cm^2

$\rho_2 = .10, .32, 1.0$ 10 Ω-cm CdS

or

$n_2 = 6.2 \times 10^{17}, 2.0 \times 10^{16}, 6.2 \times 10^{16},$

6.2×10^{15} cm^{-3}

the j_L variation with voltage. It doesn't include the j_{LO} variation with V. It is also based on the constant space charge approximation for F_2.

In Fig.14 are three I-V curves for the same cell (372D) taken with roughly the same photon fluxes but differing in the spectral content of the light. Curve (1) is the usual tungsten iodide AM1 simulation which is known to be deficient in the blue portion of the spectrum as compared to actual sunlight. Curve (2) is for blue rich light with roughly the same photon flux obtained by use of a Fresnel lens and a filter which passes only light with λ in the 4800-6000 Å range. Curve (3) was obtained with red rich light using the Fresnel lens and a filter which passes only light with $\lambda > 6600$ Å. Tables 11 and 12 give the relevant data. Note that V_{oc} is essentially the same for each case as is j_L at reverse bias. These curves illustrate the effects discussed previously[4] in connection with Eq. (6). The field F_2 can be decomposed into a light induced term which is essentially independent of voltage and a voltage dependent term i.e.

$$F_2 = F_L + [2\ (V_D^* - V)\ N_D^*\ q/\varepsilon\varepsilon_0]^{\frac{1}{2}} \tag{14}$$

Since F_L is strongly dependent on spectral content as demonstrated by photocapacitance versus wavelength and spectral response without bias light, the use of Eqs. (14) (6) in Eq. (3) can account for the curves in Fig. 14.

The blue rich light enhances the fill factor of the cell in Fig. 14 by 0.03. This would show up in plots of the type seen in Fig. 11 as shift in the curves and a lower intercept. The magnitude of $\Delta(FF)_0$ depends on F_L which depends on the density of centers in CdS near the junctions that can be ionized, and the intensity and wavelength of the

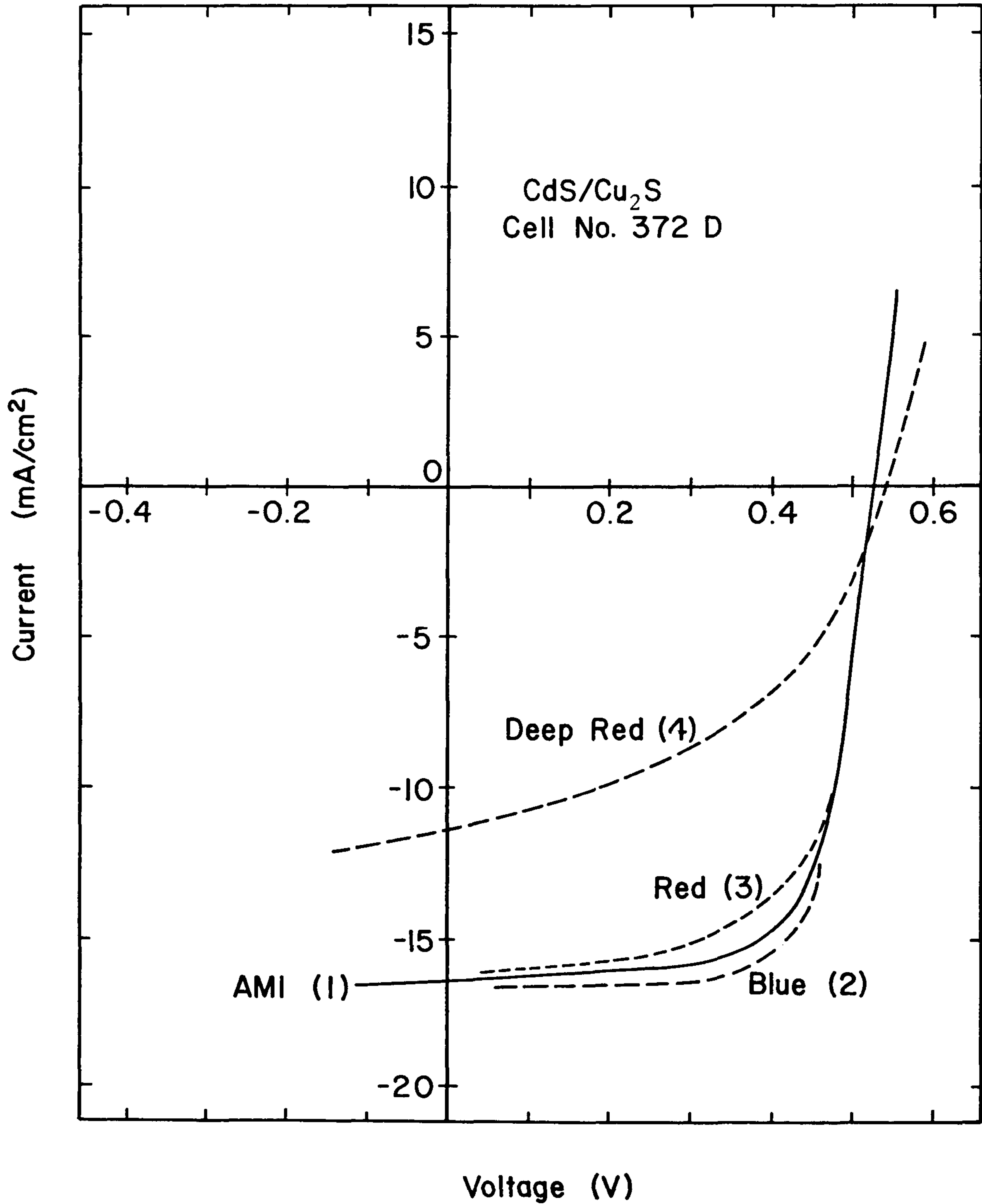

Figure 14. Current-voltage curves taken with filtered light as indicated in Tables 11 and 12.

Table 11

Color Filters Used

Dow Corning #	Approximate Color	Pass Band
4-94	Blue (B)	$\lambda < 5900$ Å
3-68	Orange (O)	$\lambda > 5400$ Å
2-73	Red (R)	$\lambda > 5800$ Å
2-64	Deep red (DR)	$\lambda > 6600$ Å

Table 12

I-V Results Using Color Filters on Cells

Cell #	Filter #	J_L (ma/cm^2)	V_{oc} (V)	J_{sc} (ma/cm^2)	FF (%)
372D	None	16.3	.510	16.3	69.4
	4-94 (B)	"	.500	"	71.7
	2-73 (R)	"	.516	"	63.1
	2-64 (DR)	"	.516	11.3	44.9
455B2-2	None	18.6	.509	18.6	67.9
	4-94 (B)	"	.497	"	71.0
	3-68 (O)	"	.510	17.3	56.5
	2-73 (R)	"	.511	16.7	51.4
482A1	None	10.4	.438	10.4	51.0
	3-68 (O)	10.3	.495	10.3	58.5
	2-73 (R)	"	.500	"	59.6
	2-64 (DR)	"	.518	"	61.5

light reaching the CdS. Since the light must pass through the Cu_2S to reach the CdS, the thickness of the Cu_2S layer can play a role in determining the ultimate value of $\Delta(FF)_0$. Since the thickness of the Cu_2S also affects the fill factor of cells through the series resistance term an optimum thickness for fill factor and short circuit current must be determined. (In the high current state after H_2-Ar heat treatment j_L is found to increase with Cu_2S thickness for dip times studied up to this time.)

Additional spectral studies are given in Table 12, for cells with somewhat different thermal histories. Cell 372D was a cross gridded cell that had undergone extensive heat treatments. Cell 455B2-2 is a more representative cell for present processing. It has an 80 line per inch evaporated grid with bus bars and a SiO antireflection coating. Cell 482A is also an evaporated grid cell (60 lines/inch) but it was measured prior to any heat treatments except those necessary for gridding and Cu_2S formation.

The improvement in fill factor under short wavelength light has been discussed above in terms of the increase in the light induced field at the Cu_2S-CdS interface. For cells with little heat treatment, a very narrow space charge region exists, and tunneling through the narrow top region can occur, particularly in the presence of light which enhances the field by ionizing deep levels near the junction. The long wavelength light will cause less field enhancement and hence less tunneling. Both V_{oc} and fill factor will thus be improved as seen for cell 482A1. Further heat treatment of the cell will compensate the CdS tailoring the potential at

interface so that less tunneling occurs. Further studies of these phenomena are planned.

In our discussion of band bending in Cu_2S after H_2-Ar heat treatment we suggested that hole densities as low as $2 \times 10^{17}/cm^3$ might be present in Cu_2S. From the resistivity one has $\rho = 6.25 \times 10^{18}/\mu p$, where μ is the mobility of the holes in Cu_2S. For ρ values of 0.2 Ω-cm which we deduced earlier for the high resistance state one has

$$p = \frac{3.1 \times 10^{19}/cm^3}{\mu} \quad (14)$$

The key question is the value of μ. Values reported in the literature for p in the 10^{18} - $10^{21}/cm^3$ range give $\mu \simeq 2$ - 30 cm^2/V-sec.[5] However, recent work[6] on single crystals indicate values as high as 800 cm^2/V-sec in nearly stoichiometric material, with μ rising very rapidly as stoichiometry is approached. The plot of resistivity versus stoichiometry shows a region in which the resistivity remains almost constant as p falls. Hence, p may be changing an order of magnitude while ρ remains unchanged, if μ is changing rapidly. This effect may account for the observation of only small resistance changes being noted while features of the I-V change significantly. A rise in μ is to be expected if the dominant scattering mechanism shifts from ionized impurity scattering for $p > 10^{18}/cm^3$ to lattice scattering for $p < 10^{18}/cm^3$.

c) Shunt Resistance

In some cells low shunt resistances, on the order of 1500 Ω-cm^2, have been noted. The change in FF due to shunt resistance is given by

$$\Delta(FF)_{R_{sh}} = -\frac{V_{mp}}{AR_{sh}} \frac{V_{mp}}{j_{sc}V_{oc}} \quad (15)$$

The change is inversely proportional to intensity through j_{sc} and can invalidate low intensity points in plots of the type shown in Fig.11. At AM1 a 1500 Ω-cm^2 shunt resistance reduces FF by $\sim$ .01.

In summary the fill factor is determined by a number of factors, the major loss mechanisms are:

a) Series resistance due to resistivity of Cu_2S layer;

b) Voltage dependence of j_L due to stoichiometry caused band bending in Cu_2S, and due to the spectral and intensity dependent field at the junction,

c) Low shunt resistance - due probably to edge effects.

2. Diffusion Coefficient Limiting Rate of Cu_2S Formation

We have previously derived an expression for the equivalent thickness of Cu_2S formed on CdS by the wet dip technique. The expression obtained was[7]

$$\bar{d}(t) = T\, C_1\, t^{\frac{1}{2}} + \frac{C_1 C_2}{r}\, t$$

where T is the ratio of the true surface area to the geometrical area of the Cu_2S, C_1 is related to the diffusion coefficient of the rate limiting process in the formation of Cu_2S from CdS, and t is the dip time. In a previous study[8] data on unetched and etched material is given as a function of dip time. In Fig. 15 we have plotted the data and drawn

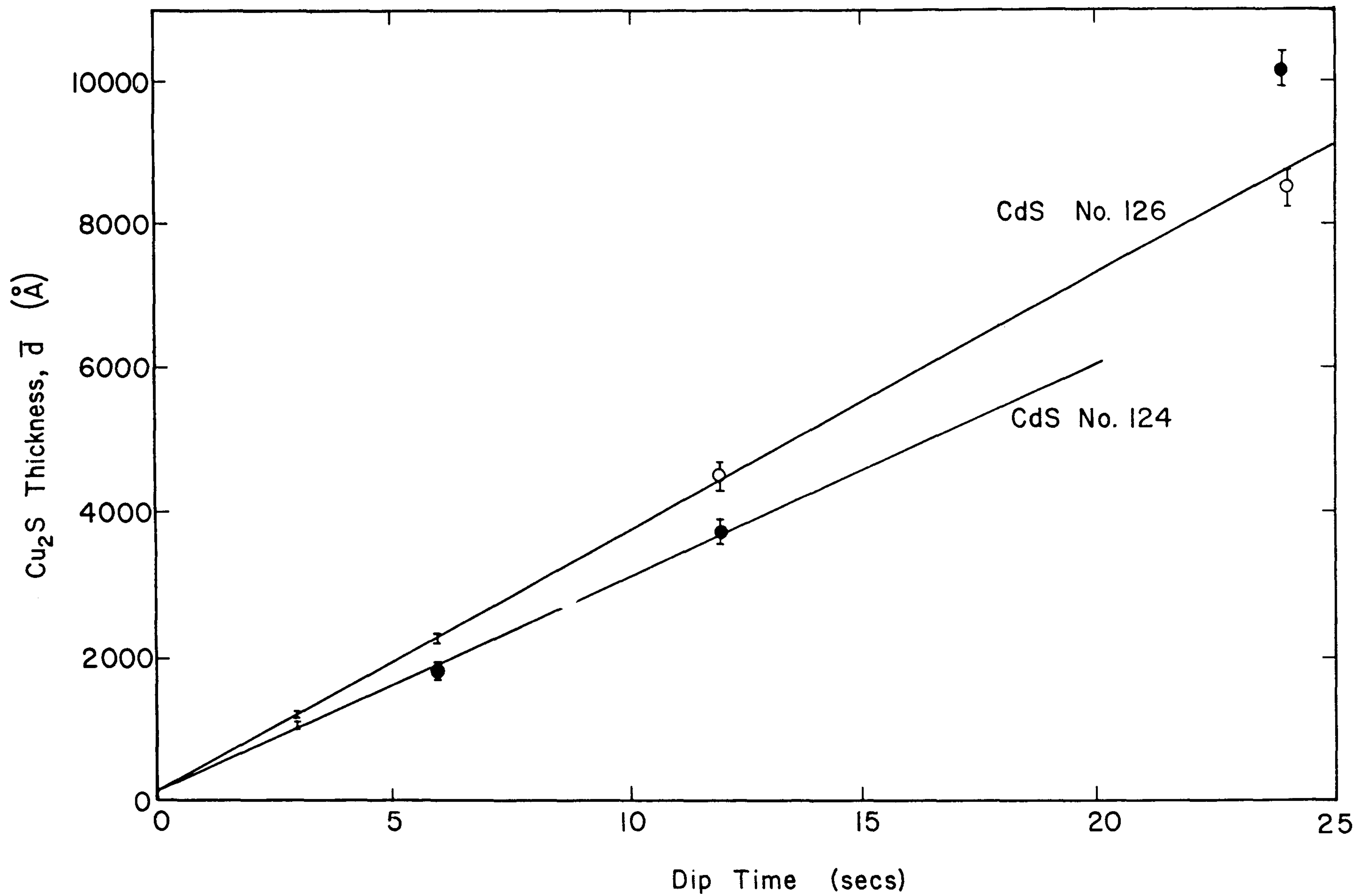

Figure 15. Plot of Cu_2S thickness as a function of reaction time in cuprous chloride solution.

straight lines through the points. For substrate 124 (unetched) the slope of the straight line is ∿ 300 Å/sec, and for 126 (3 sec etch) the slope is ∿ 344 Å/sec. Using the value from the substrate 124 we obtain

$$\frac{C_1 C_2}{r} = 300 \text{ Å/sec} = 3 \times 10^{-6} \text{ cm/sec}$$

Since one of the assumptions in the derivation of (2-1) was that $C_2 = gC_1$. Where g is a constant, we can write

$$C_1^2 = 3 \times 10^{-10} \text{ cm}^2/\text{sec} \ \frac{r}{g}$$

where r is in μm.

From etch studies r ∿ 1 μm, and from the depth of penetration of Cu_2S down grain boundaries g ∿ 50. Hence, $C_1^2 \approx 6 \times 10^{-12}$ cm^2/sec.

Since the diffusion coefficient of the rate limiting step is directly proportional to C_1^2 it may be possible to determine whether components in the dip limit the process or diffusion of Cu or Cd in the Cu_2S limits the process.

3. (CdZn)S/Cu_2S Cell Analysis

Studies of cells prepared on various compositions of $Cd_{1-x}Zn_x$-Cu_2S were carried out using capacitance and I-V analysis.

a) V_{oc} Studies

As reported previously the open circuit voltage of these cells show a marked time dependence. However, by waiting a sufficient length of

time (~ 30 minutes), steady state values are achieved. In Fig. 16 V_{oc} (steady state) versus Zn composition is plotted with j_{sc} values normalized to j_{sc} = 10 mA/cm^2, i.e.

$$V_{oc}\ (10\ mA/cm^2) = (V_{oc})_{observed} + \frac{kT}{q}\ \ell n\ \left(\frac{10\ mA/cm^2}{j_{sc}}\right)$$

The Cu_2S layer was prepared by dry process and was ~ 2000 Å thick. Table 13 gives pertinent data on the cells.

Table 13

I-V Results for $Cd_{1-x}Zn_xS$ Dry Dip Cells

Cell	% Zn	j_{sc} mA/cm^2	$V_{initial}$	V_{oc} Steady State	V_{oc} at 10 mA/cm^2
369D1	27	0.82	.680	.665	.730
369D3	19	3.31	.652	.625	.654
369D5	11	6.02	.640	.580*	.593

*Still decaying after 30 minutes

The slope of the line in Fig. 16 is ~ 0.9 V. According to the theory(9) of V_{oc} in mixed $Cd_{1-x}Zn_xS$ cells the slope of the line should equal $\chi_{CdS} - \chi_{ZnS}$. The listed χ values are χ_{ZnS} = 3.9 eV while χ_{CdS} = 4.0 - 4.8 eV. Hence, our observed value is within the range expected.

b) Capacitance Studies

The capacitance of Cu_2S-$Cd_{1-x}Zn_xS$ cells were studied as a function of Zn composition and also as a function of etch time. Fig.17 gives C/A as a function of Zn composition for dry processed cells, with d_{Cu_2S} =

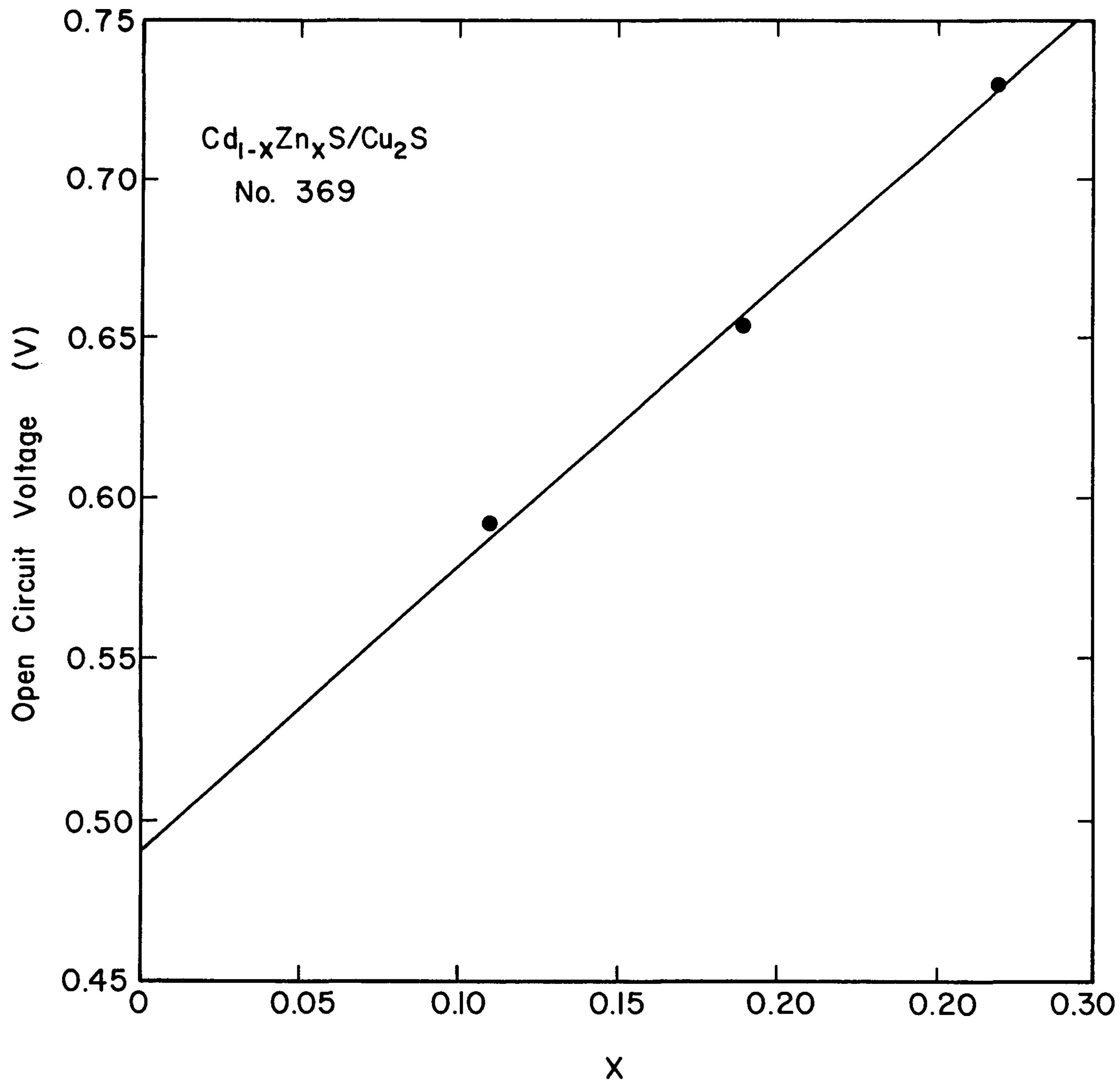

Figure 16. Open circuit voltage normalized to j_L = 10 mA/cm^2, as a function of Zn content in $Cd_{1-x}Zn_xS$-Cu_2S solar cells.

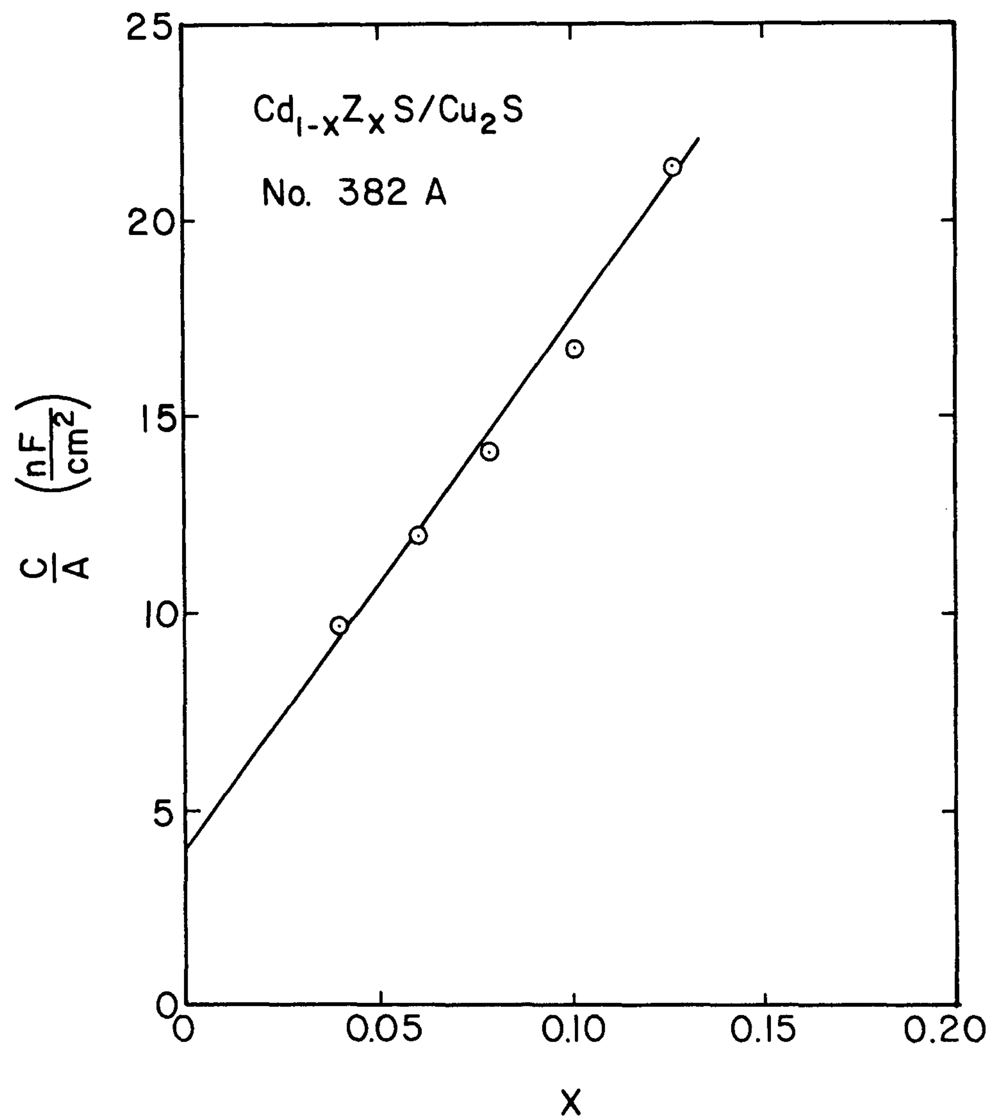

Figure 17. Capacitance as a function of Zn content in $Cd_{1-x}Zn_xS-Cu_2S$ solar cells.

~ 3000 Å. The increase of C with Zn composition is surprising since generally the resistivity is higher in Zn rich material and the capacitance would be expected to fall with increasing Zn content. Since the capacitance of cells is usually determined by the width of the compensated region, associated with the diffusion of Cu into CdS (or $Cd_{1-x}Zn_xS$), the above result suggests that Cu diffusion is less in Zn rich material. The fact that the lattice constant falls with increasing Zn, is consistent with this explanation of the result.

In Fig. 18 the capacitance and short circuit current of dip processed cells with Zn % in the 15.5-16.8 range are plotted. The fall in both C/A and j_L with etch time is contrary to observations in CdS cells. A possible explanation of these results may be in the extremely high resistivity of the $Cd_{1-x}Zn_xS$ in these cells. The resistivity of substrate 426 was so high that the usual In dot method did not yield consistent results. The high resistivity material coupled with a rough surface may result in highly compensated regions with low electric field at the junction. Both the low j_{sc} and low C/A values would then follow.

Wet processed mixed sulfide cells have had a number of difficulties. The most serious are, low open circuit voltage in many instances and severe time dependence of the open circuit voltage. These effects are most likely related to grain boundary penetration of Cu_2S and the diffusion of Cu into $Cd_{1-x}Zn_xS$.

c) Heat Treatment Studies

One of the difficulties in optimizing the mixed sulfide cells is achieving an adequate heat treatment procedure. The experimental

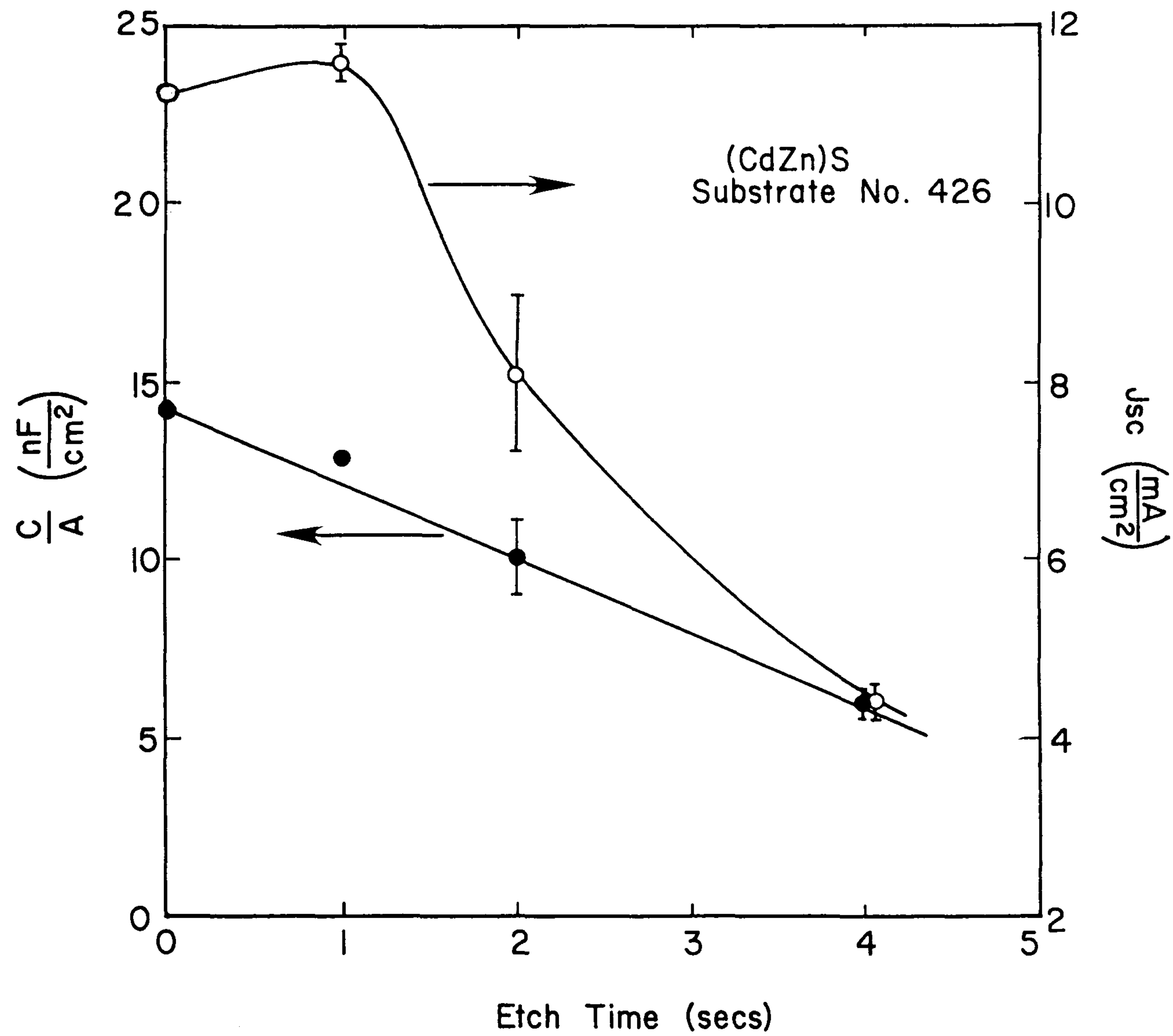

Figure 18. Capacitance and short circuit current density as a function of etch time for $Cd_{1-x}Zn_xS$-Cu_2S solar cells.

difficulties arise from the fact that the cells vary in both Zn content and resistivity. The heat treatments serve at least two important functions in determining cell characteristics. The first involves the creation of a compensated region in the CdZnS layer near the junction by the diffusion of Cu into this layer. As we have indicated earlier, the ionization by light of the Cu levels is important to both the short circuit current and fill factor of the cell. As we suggested in our discussion of C/A as a function of Zn content Cu may diffuse less readily with increasing Zn content. The second effect of heat treatment is the reduction of any Cu_2O on the surface of the Cu_yS layer to Cu with the incorporation of this Cu into the layer increasing its stoichiometry. The higher stoichiometry Cu_yS leads to both higher series resistances and higher short circuit currents. However, it can reduce both fill factor and open circuit voltage.

In Table 14 we list some of the characteristics of cells and their dependence on heat treatment. The cells, in their production, experience significant heat treatments during the deposition of gold grid lines and the lamination of the cross grid. The capacitance values obtained are similar to those of CdS cells despite the fact that the resistivity of the CdZnS is roughly a factor of 10 higher than that of CdS. If the capacitance were controlled by the shallow donor densities rather than the compensated density with the uncovering of deeper levels, these facts would imply that the mobility in the CdZnS layers was roughly a factor of 10 less than in CdS. If the mobility were indeed significantly lower in the $Cd_{1-x}Zn_xS$ material then short circuit currents would be lower through Eq (6). Further study of the capacitance of the cells and also Schottky

Table 14

Heat Treatment Study on Mixed Sulfide Solution Reacted Cross Gridded Cells (40 x 40 Lines Per Inch)

Cell	% Zn	ρ (ohm-cm)	V_{oc}	j_{sc} (mA/cm²)	FF	$\frac{C}{A}$ ($\frac{nF}{cm^2}$)	Etch Time (Sec)	Conditions	Measurement Conditions
413A-2	7.4	∿ 50	0.611	8.61	0.679	12.24	0	Production	Sweep I-V
			0.524	8.61	0.708	12.24	0	Production	Steady State I-V
			0.605	12.63	0.651	9.19	0	5 hr. at	Sweep I-V
			0.515	12.41	0.642	9.19	0	170°C in H_2-Ar	Steady State I-V
413E4	5.3	∿ 30	.559	11.42	0.527		1 sec	Production	Sweep I-V
			.531	11.42	0.555		1 sec	Production	Steady State I-V
			.590	15.25	0.585		1 sec	5 hr. at 170°C in H_2-Ar	Sweep I-V

diodes should help to determine whether the mobility is a problem in the mixed sulfide cells.

d) Apparent Energy Gap - Schottky Diode Study

The apparent energy gap in the mixed sulfides as deduced from peaks in the spectral response of the cells and photocapacitance has been studied further. One possible cause of the peak occurring at higher energies than that indicated by x-ray and optical data was inhomogeneous Zn concentration near the junction, due to either (1) Zn enrichment of the depletion region during the formation of Cu_2S or (2) inhomogeneous deposition and/or growth of the $Cd_{1-x}Zn_xS$ layer.

The Zn enrichment hypothesis was tested by comparing the peaks in spectral response of Au-$Cd_{1-x}Zn_xS$ Schottky diodes prepared using $Cd_{1-x}Zn_xS$ with and without Cu diffusion. Copper diffusion was achieved by solid state reaction with CuCl to produce 1000 Å of Cu_2S. During this reaction some copper diffusion into the (CdZn)S should occur. Following the reaction the Cu_2S was stripped off to expose the (CdZn)S surface.

The peaks in the photocapacitance are associated with free exciton absorption in the mixed sulfide. The high absorption coefficient limits the area being studied to within 10^{-5} cm of the Au interface, and it is in this region that differences in Zn content would be evident. Table 15 shows the results obtained.

Table 15

Apparent Energy Gaps Deduced from Spectral Response of Schottky Diodes on Cu-Diffused and Undiffused $Cd_{1-x}Zn_xS$

Diode #	% Zn	E_g (Cu-diffused)	E_g (Undiffused)
451-1	29.2	2.82 ± 0.03 eV	2.82 ± 0.03 eV
451-2	24.0	2.77 ± 0.02	2.77 ± 0.02
451-3	15.0	2.65 ± 0.02	2.65 ± 0.02
441	0	2.49 ± 0.02	

The fact that the results are identical for Cu diffused and undiffused diodes seems to rule out Zn enhancement due to the formation of the Cu_2S layer. Inhomogeneous deposition or growth still remains as a possible explanation of the effect. An additional possibility is the existence of a high density of native hole traps in the mixed sulfides, that limits the distance from the junction from which generated holes can reach the junction and contribute to the current. This mechanism would restrict the wavelength which contribute to short circuit current to those

absorbed very close to the junction. The response of the Schottky diode acting as a solar cell should go as $\alpha L_h/(L_h\alpha + 1)$, where L_h is the diffusion length for holes; $L_h = (kT\ \mu_h\ \tau_p/q)^{1/2}$. The mobility of holes in ZnS is less than that in CdS. Hence, with increasing Zn content μ_h will fall. Other effects such as the dependence of L_h on field in the space charge region, changes in resistivity with Zn content, and possible changes in barrier height with Zn content make any model of this effect highly speculative at this time.

4. Capacitance Saturation Effect

The capacitance of cells decrease with heat treatment due to the compensation of the CdS by Cu diffusion from Cu_2S. In many instances, the capacitance decreases to a saturation value of $C/A \sim 3 \times 10^{-9}$ F/cm^2 corresponding to a width of the space charge region of ~ 3 µm. This effect has been seen in capacitance studies[10] of Cu diffusion in CdS. Such an effect can be explained most readily with the band diagram shown in Fig. 19 which we have used previously in discussing the cross-over of dark and light I-V curves.[4] The voltage V_{D_1} between the Cu compensated and the uncompensated CdS depends upon the degree of compensation caused by the Cu diffusion. The degree of compensation is controlled by the temperature of the heat treatments, the solubility of Cu in CdS, and the densities and energy levels of various defects in the CdS. In Table 16 we have listed the energy levels which have been reported[11] to be present in evaporated CdS samples. The identity of the various levels is not known definitively, but assignment of most likely identities has been made.[12] The 0.05, 0.14, and 0.25 eV levels are seen most frequently in cadmium-rich samples and are assumed to be various types of sulfur vacancies. The 0.61 center is

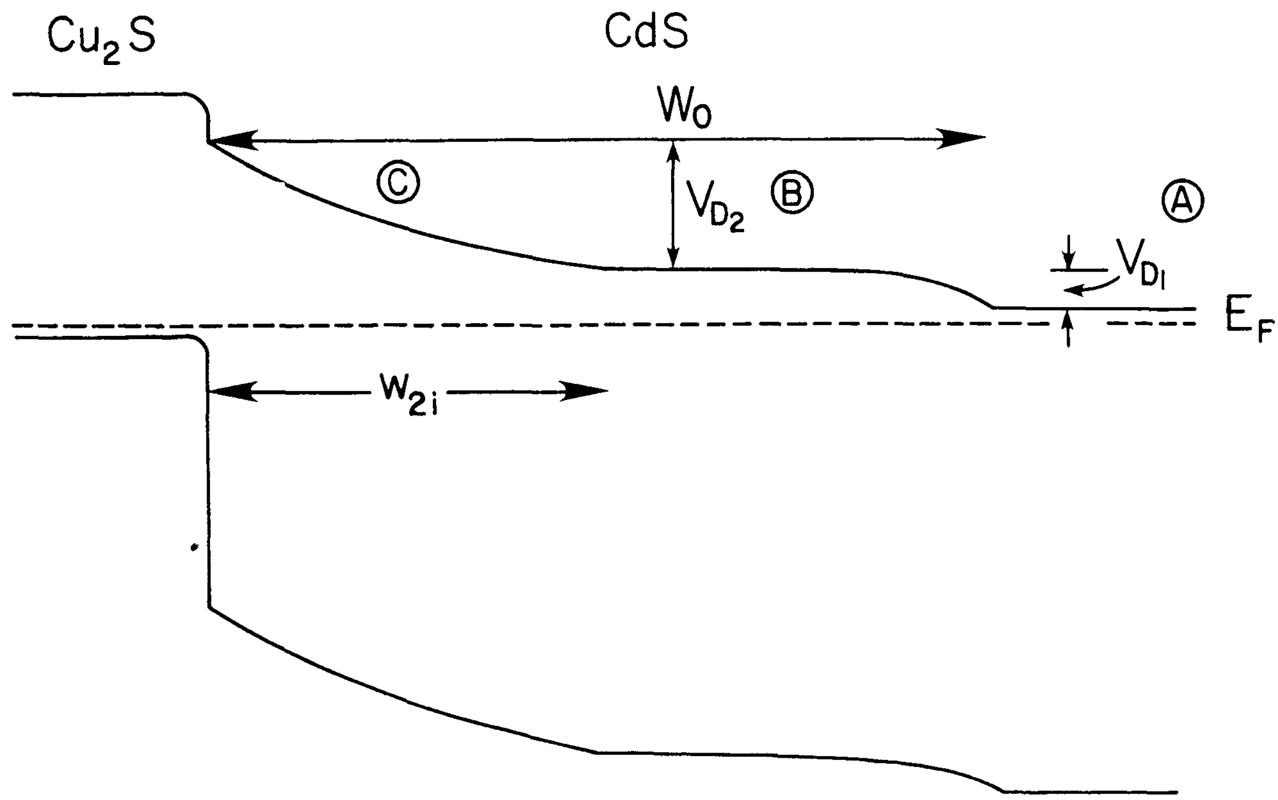

Figure 19. Band diagram of CdS/Cu_2S solar cell illustrating compensated region of CdS.

seen in sulfur-rich material. The 0.41 and 0.82 levels usually occur together, and are present in both sulfur-rich and cadmium-rich samples, and hence maybe complexes of cadmium and sulfur vacancies in nearest neighbor sites.

The solubility of Cu in CdS is given by[13]

$$[Cu] = 6.6 \times 10^{22} \exp \left(-\frac{0.505 \text{ eV}}{kT}\right)$$

Hence, the highest temperature seen by the cell will determine the concentration of Cu in CdS. For a 200°C temperature [Cu] = 2.8 x $10^{17}/cm^3$ is expected. Since [Cu] is an acceptor, the position of the Fermi level in the compensated region is determined by the condition that [Cu] = $\Sigma_i N(E_i)_{E_i > E_F}$ where $N(E_i)$ is the density of centers with energy E_i. We expect the Fermi level will lie at one of the levels listed in Table 16.

If we take the 0.26 eV level as the depth of the Fermi level in region (B) of Fig. 19, the electron density at 300°K in this region is given by

$$n = N_{c_2} \exp(-0.26/kT) \simeq 9 \times 10^{13}/cm^3$$

Assuming $qV_{D_2} = \phi - .26 = 0.74$ eV the expected width controlling capacitance w_{2i} is 3.06 x 10^{-4} cm and the capacitance 2.89 nF/cm^2. These values correspond closely to the saturated capacitance seen in cells.

This strongly suggests that in cells made at Clevite and also those presently being made, the 0.26 eV levels exist in high density, or the sum of all levels at 0.26 eV or higher is sufficient to accomodate the density of Cu centers which enter into CdS during the heat treatments. The calculation above gave a Cu density of $\sim$ 2.8 x $10^{17}/cm^3$. The resistivity

of CdS in cells ranges from 0.1-10 ohm-cm and with a mobility of ∿ 50 cm^2/V-sec, values of n in uncompensated material could range from 10^{16}-10^{18}/cm^3. The saturation effect is more likely to occur in higher resistivity material.

Table 16

Trap Levels in CdS, in eV

Trap Levels (eV)
.05 - .08
.14 - .16
.24 - .26
.41 - .45
.61 - .63
.82 - .83

5. Preliminary Results of Dark I-V Drift Measurements on CdS and Mixed Sulfide Cells

Experiments have resumed on investigating the behavior of the cell under forward bias in the dark. With a forward current turned on and maintained by a constant current supply the voltage across the cell is monitored as a function of time. While the voltage ultimately decays to a value corresponding to a point on the light I-V curve shifted by I_L, the initial value when the current is turned on can be much higher depending on the treatment given the cell and its immediately past electrical condition.[4]

Measurements of this voltage decay on a few mixed sulfide cells (369 series) showed a combination of smooth decay and step-like drops in voltage; a typical result is shown in Fig. 20. The position and size of

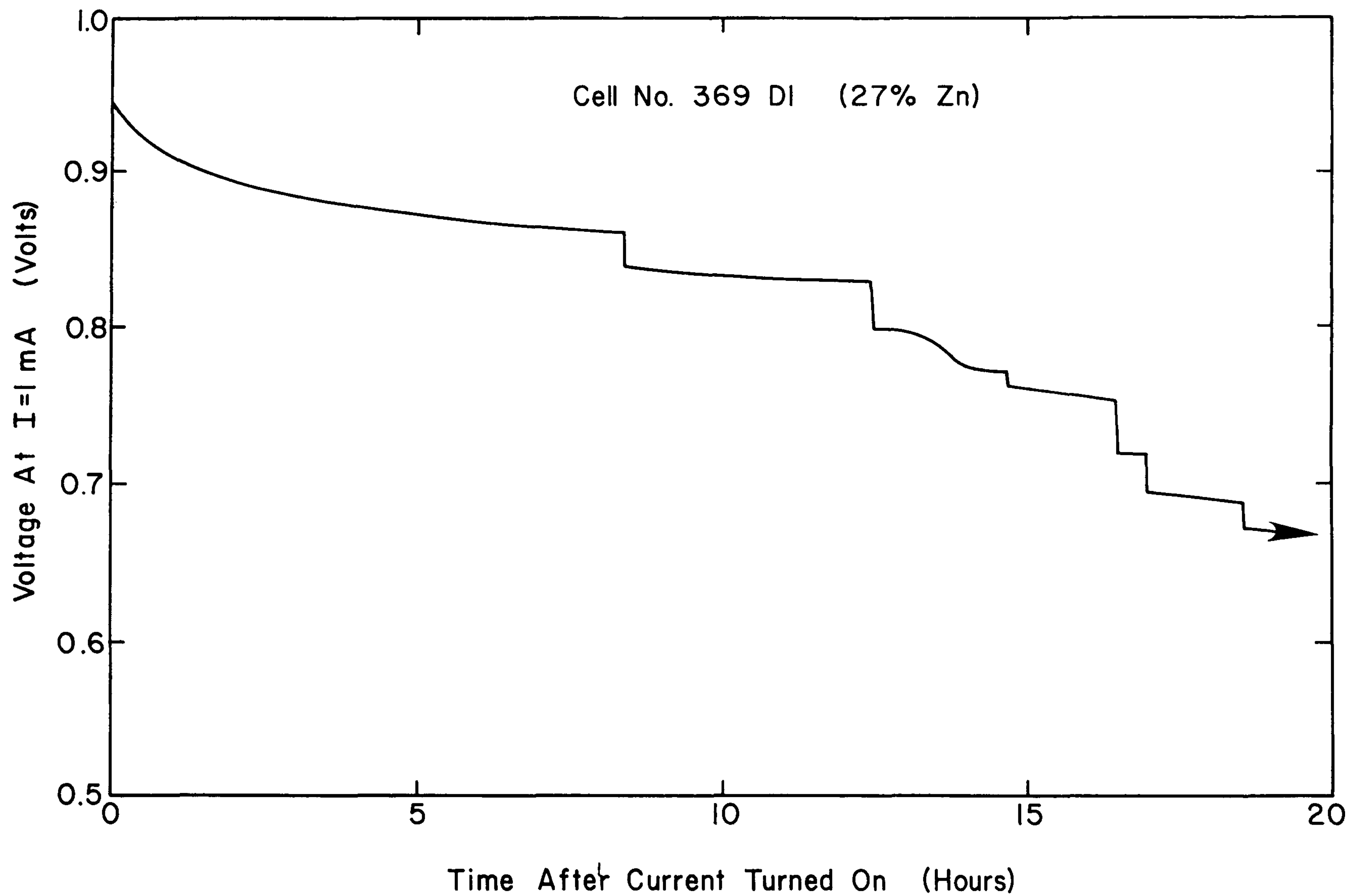

Figure 20. Dark voltage decay as a function of time for a $(CdZn)S/Cu_2S$ solar cell.

of the steps was not reproducible from run to run. The further study of this behavior has been postponed in favor of experiments on CdS/Cu_2S cells.

The CdS cells studied so far show a smooth decay with a total equilibrium time of $\sim 6.5 \times 10^4$ sec. (18 hrs.). The decay is not a simple exponential but may be a composite of exponentials. After the cell achieves a steady-state voltage for a given current, the voltage overshoots its equilibrium value if the current is increased suddenly and undershoots the equilibrium value (with subsequent decay up to it) if the current is decreased suddenly.

Other preliminary work has shown that exposure to infrared radiation before the current is imposed causes a change in the voltage versus time behavior; this is illustrated in Fig. 21. A decrease in the AM1 open-circuit voltage of cells which have been in forward bias in the dark for many hours ($\gtrsim 50$) has also been seen.

Further experimental work and theoretical modeling of the observed behavior is proceeding.

6. Time Dependent V_{oc}

Preliminary measurements have been made to determine the origin of the long time constant behavior of the I-V characteristics in the mixed sulfide cells.

The measurements made so far have shown:

(1) Unstable V_{oc} behavior is not only a characteristic of the mixed sulfide cells, but also occurs for some wet and dry processed CdS cells.

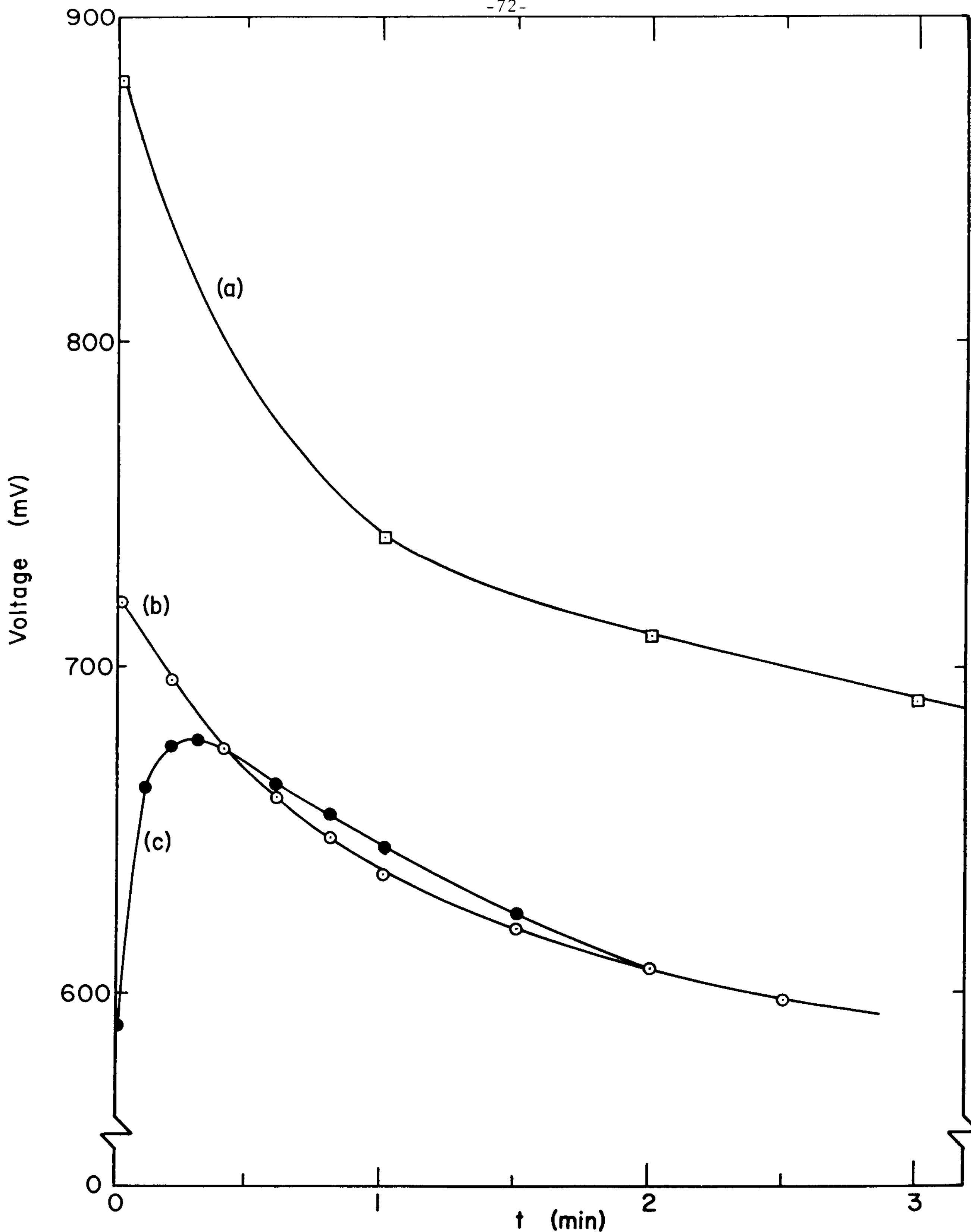

Figure 21. Dark voltage decay as a function of time in a $CdS\text{-}Cu_2S$ solar cell under various conditions. (a) Initial decay curve during first few minutes, (b) After having reached saturation voltage and being shorted for five minutes in dark, (c) Same as (b) but with the cell exposed to infra light during shorting time.

(2) The magnitude of this time dependent behavior is a function of the illumination intensity and spectra.

Since the time dependent V_{oc} phenomena occurs on some CdS cells and not on others, the differences between the two types of cells has to be identified.

References

1. Progress Report E(49-18)-2538 PR76/2, May 1977.

2. A. Rothwarf and A. M. Barnett, IEEE Trans. on Electron Device, ED-24, 381-387, (1977).

3. A. Rothwarf, Light Generated Current Densities in the CdS/Cu_2S Solar Cell, NSF/RANN/AER72-03478/TR/75/3.

4. Progress Report E (49-18)-2538 PR76/1, January 1977.

5. A. Rothwarf and K. W. Böer, Progress in Solid State Chemistry, 10, 71, 1975.

6. G. Z. Idrichan and G. P. Sorokin, Inorganic Materials, 11, 1449 (1975).

7. Progress Report NSF/RANN/AER72-03478 A04 FR76, March 1977, p. 35.

8. Progress Report NSF/RANN/AER72-03478 A04 PR75/4, March 1976, p. 33.

9. Ref. 8, p. 80.

10. L. R. Shiozawa, F. Augustine, G. A. Sullivan, J. M. Smith III, and W. R. Cook, Jr., Clevite Final Report ARL69-0155, October 1969, p. 44-53.

11. K. H. Nicholas and J. Woods, Brit. J. Appl. Phys. 15, 783 (1964); G. A. Marlor and J. Woods, Brit. J. Appl. Phys. 16, 1449 (1965); U. Büdet and G. T. Wright, Brit. J. Appl. Phys. 16, 1457 (1965); H. W. Brandhorst, Jr., F. L. Campora and A. E. Potter, Jr., J. Appl. Phys. 39, 6071 (1968).

12. J. Woods and K. H. Nicholas, Brit. J. Appl. Phys. 15, 1361 (1964).

13. Ref.10, p. 50-55.

Appendix A

LIST OF RESEARCH CONTRIBUTORS

Dr. John D. Meakin, Associate Director, Principal Investigator

Dr. Allen M. Barnett, Director

Dr. Bill N. Baron, Associate Scientist

Dr. Charles E. Birchenall, Distinguished Professor of Metallurgy

Dr. Larry C. Burton, Scientist

Dr. Walter E. Devaney, Research Associate

Mr. Thomas L. Hench, Research Assistant

Ms. Leslie M. Kilgren, Research Associate

Mr. Steven Lorenz, Electronics Engineer

Mr. George Miller, Senior Laboratory Technician

Dr. Roy L. McCullough, Professor of Chemical Engineering

Mr. Patrick Mulvihill, Graduate Student

Dr. Larry D. Partain, Assistant Professor of Electrical Engineering

Mr. James E. Phillips, Research Associate

Dr. Allen Rothwarf, Senior Scientist

Dr. Joseph Sansregret, Research Associate

Mr. Stephen Shea, Graduate Student

Dr. George Storti, Research Associate

Mr. David Brindle, Instrument Technician

Mr. David Cowgill, Senior Design Machinist

Ms. Gwendolyn A. Howk, Senior Research Technician

Mr. Thomas Lovett, Undergraduate

Ms. Maryanne Powers, Senior Research Technician

Mr. Robert Wieland, Research Technician

Mr. Walter Willing, Undergraduate

Mr. David Potts, Graduate Student

Ms. Sandra Lynn Matthews, Technical Secretary

*U.S. GOVERNMENT PRINTING OFFICE: 1978-740-306-9485. Region 4.